applied sciences

MDPI

Review

Fractal Metasurfaces and Antennas: An Overview for Advanced Applications in Wireless Communications

Francesca Venneri [1,2,*], Sandra Costanzo [1,2,3] and Antonio Borgia [1,2]

[1] Dipartimento di Ingegneria Informatica, Modellistica, Elettronica e Sistemistica (DIMES), Università della Calabria, Via P. Bucci 41D, 87036 Rende, Italy; costanzo@dimes.unical.it (S.C.); antonio.borgia@dimes.unical.it (A.B.)
[2] CNIT (Consorzio Nazionale Interuniversitario per le Telecomunicazioni), 43124 Parma, Italy
[3] ICEmB (Inter-University National Research Center on Interactions between Electromagnetic Fields and Biosystems), 16145 Genoa, Italy
* Correspondence: venneri@dimes.unical.it

Abstract: This paper provides an overview of fractal antennas and metasurfaces, exploring their design principles, performance, and applications. Fractal antennas, incorporating self-similar geometric shapes, offer several advantages, such as their multiband operation, compact size, and improved performance. Metasurfaces, on the other hand, are two-dimensional structures composed of subwavelength unit cells and are designed to achieve advantageous and unusual electromagnetic properties by enabling precise control over electromagnetic waves. This paper discusses the fundamental concepts of fractal antennas and metasurfaces, compares their characteristics, and presents the latest advances in research. Additionally, it highlights applications in wireless communications, energy harvesting, sensing, and beyond.

Keywords: fractal antennas; reflectarray; metasurfaces; microwaves; metamaterial absorbers

Citation: Venneri, F.; Costanzo, S.; Borgia, A. Fractal Metasurfaces and Antennas: An Overview for Advanced Applications in Wireless Communications. *Appl. Sci.* **2024**, *14*, 2843. https://doi.org/10.3390/app14072843

Academic Editor: Piotr Gas

Received: 16 February 2024
Revised: 12 March 2024
Accepted: 26 March 2024
Published: 28 March 2024

1. Introduction

Fractals are mathematical objects exhibiting self-similarity properties at different scales. This means that when you zoom in/out on a fractal shape, each part of it looks very similar to the whole; i.e., similar geometric patterns or structures are repeated at different levels of magnification (see the fractal examples in Figure 1). Most fractals have intricate, detailed, and infinitely complex shapes.

The fractal concept was introduced by the mathematician Benoit B. Mandelbrot in the 1970s [1], although the origins of fractal geometry can be traced back to earlier works by various mathematicians, such as Cantor (1870) [2], von Koch (1904) [2], Sierpinski (1915) [3], Julia (1918) [4], Fatou (1926) [5], and Richardson (1953) [2].

Mandelbrot investigated the relationship between fractals and nature by introducing new types of fractals to model more complex structures, such as trees, mountains, and coastlines [6]. He coined the term "fractal" from the Latin adjective "fractus", which means "broken" or "fractured", i.e., made up of broken or irregular fragments, to describe irregular and fragmented geometrical shapes that could not be classified using traditional Euclidean geometry. Furthermore, he developed mathematical models and algorithms to generate and study fractals, leading to the creation of the famous Mandelbrot set [7], being perhaps the most well-known and visually fascinating fractal shape, with its intricate and infinitely repeating patterns (see Figure 1d).

Mandelbrot's work not only had an impact on mathematics, but also found applications in various fields, such as physics, computer graphics, biology, economics, and art. Indeed, fractals have numerous innovative applications in various fields due to their ability to model and represent complex and self-similar structures. For instance, they have been

widely used in the following application fields, which are just a few examples of their wide-ranging applications:

- computer graphics and animation, to generate realistic and visually appealing natural landscapes, trees, clouds, and textures;
- data compression techniques, to reduce the size of digital files;
- image and signal processing, to extract features from images, detect patterns, and provide efficient methods for image compression and reconstruction;
- biology, to describe the growth of plants and the organization of neurons in the brain;
- antenna theory and metamaterials, to design compact/multiband antennas and innovative metasurfaces.

Currently, fractal geometry continues to find new and innovative uses across various scientific, artistic, and technological disciplines.

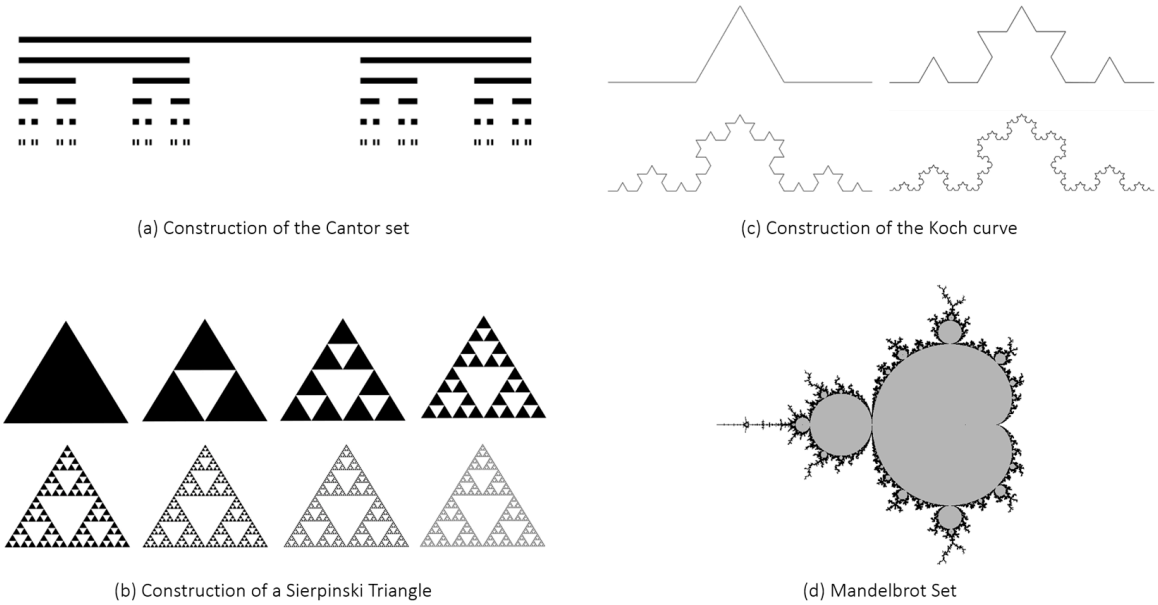

Figure 1. Examples of fractal shapes/curves: (**a**) Cantor set, (**b**) Sierpinski triangle, (**c**) Koch curve, (**d**) Mandelbrot set.

In electromagnetic (EM) technology, fractal shapes are proving very interesting for applications requiring miniaturization, from antennas to metamaterials and frequency selective surfaces (FSSs). The use of fractal geometries in conventional antennas can increase their electrical length, thus reducing the overall size of resonant structures. Moreover, the self-similar nature of fractal shapes makes them ideal for achieving multiband or broadband resonant structures. The inherent miniaturization capabilities of fractals are particularly attractive for the design of reflectarrays, phased array antennas, metamaterial absorbers, and metasurfaces for various applications. Indeed, the use of very small array elements can offer several advantages, such as the reduction in mutual coupling or the ability to work with an array lattice with very small inter-element spacing, ensuring good scanning performance and a higher level of angular stability.

For all the above reasons, fractal antennas and metasurfaces represent two fascinating research areas in the field of electromagnetics that have attracted considerable attention in recent years [8–10]. Both concepts offer unique ways to manipulate and control electromagnetic waves, leading to a wide range of applications in wireless communications, radar systems, and sensing [11,12]. Their self-similarity property enables them to be compact in size, while maintaining excellent electromagnetic responses. This compactness is particularly advantageous in space-constrained applications, such as mobile devices, RFID tags, and aerospace systems [11,12].

The use of fractal antennas and metasurfaces has the potential to significantly improve wireless communications, imaging, and radar systems by enabling compact, high-performance devices with enhanced functionalities. Furthermore, fractal geometries are increasingly used in designing microwave sensors for materials diagnostics due to their ability to operate in multiple frequency bands and their miniaturization capabilities [13–17]. Ongoing research in these areas continues to explore new designs, materials, and fabrication techniques to exploit their full potential.

The aim of this paper is to review the progress made in the study and application of fractal antennas and metasurfaces and compare existing fractal-based antennas and metasurfaces, highlighting their benefits and limitations. Finally, a comprehensive analysis of innovative reflectarrays and metamaterial unit cells is presented and the challenges and future developments of these electromagnetic structures are discussed.

This paper is organized as follows. In Section 2, several fractal antenna elements are illustrated and discussed. Some novel fractal-based reflectarray configurations are illustrated in Section 3, highlighting their performance and advantages. Fractal metasurfaces and their applications are discussed in Section 4. The conclusions are outlined in Section 5.

2. Fractal Antenna Elements

The general concept of fractal can be applied to design exotic antenna elements, offering improved and exciting levels of performance with respect to those of conventional antennas. Fractal antenna elements may have a compact size, as well as multiband and/or broadband capabilities.

The design of fractal antennas involves the reiteration of a specific geometric pattern at different scales within the antenna structure. This self-similar pattern allows us to increase the overall antenna length within a limited physical space. Furthermore, fractal radiators can achieve multiple frequency bands because different parts of the antenna are similar to each other at different scales. As a result, fractal antenna elements can be compact and multiband, offering broader frequency coverage as compared to that of traditional antennas.

The concept of fractal antennas dates back to the late 1980s. In 1986, Kim and Jaggard demonstrated the use of fractal self-similarity in antenna array synthesis [18].

In 1988, the physicist Nathan Cohen built the world's first fractal element antenna. He proposed that, by incorporating self-similar geometric shapes into the antenna's structure, it is possible to improve its performance and miniaturization skills [19,20]. In 1995, Cohen co-founded Fractal Antenna Systems Inc. to begin delivering the world's first fractal-based commercial antenna solutions [21].

In the mid-1990s, Puente et al. [22] demonstrated the multiband capability of fractals by exploiting the Sierpinski monopole and dipole behavior.

From the works of Cohen and Puente onwards to the present day, the inherent advantages offered by fractal antennas have attracted considerable interest among researchers and engineers in the telecommunications field, leading to further exploration and development of fractal antenna technology.

Nowadays, fractal antennas are used in wireless communications systems, including mobile phones, Wi-Fi routers, and satellite communications [8–12]. Indeed, their compact size, multiband operation, and efficiency make them suitable for a wide range of wireless devices and networks.

The figures below show some fractal antennas based on well-known fractal shapes, which are just a few examples of the various configurations discussed in the literature [23–28].

In particular, Figure 2a illustrates the Sierpinski monopole introduced by Puente in [26], which is able to offer multiband behavior. The Sierpinski triangle is formed by subtracting a central inverted triangle from a main triangle shape, as demonstrated in Figures 1b and 2a. This process leaves three equal triangles on the structure, each with sides half the size of the starting triangle (see Figure 1b). The same subtraction procedure can be iterated for the remaining triangles. Thus, each one of its three main parts is exactly equal to the whole object, but scaled by a factor of two, and so on. Due to these particular

similarity properties, the Sierpinski gasket can offer multiple frequency bands because different parts of the antenna are similar to each other at different scales. As illustrated in Figure 2, the Sierpinski monopole proposed in [26] offers penta-band behavior. It can be seen that each of the five subgaskets in Figure 2a (circled structures) is a scaled version of the whole structure, thus offering five different operating bands, as shown by the input reflection coefficient in Figure 2b. The figure also shows the parameters relative to each band, including the frequency values f_n ($1 \leq n \leq 5$) at the minima of the measured input return loss (L_r), the relative bandwidth (*Bwidth*), and the frequency ratio between two adjacent bands ($\delta = f_{n+1}/f_n$). Figure 2b demonstrates that the bands of the Sierpinski monopole are log-periodically spaced by a factor of two ($\delta \cong 2$), which corresponds to the same scale factor existing among similar structures on the fractal shape.

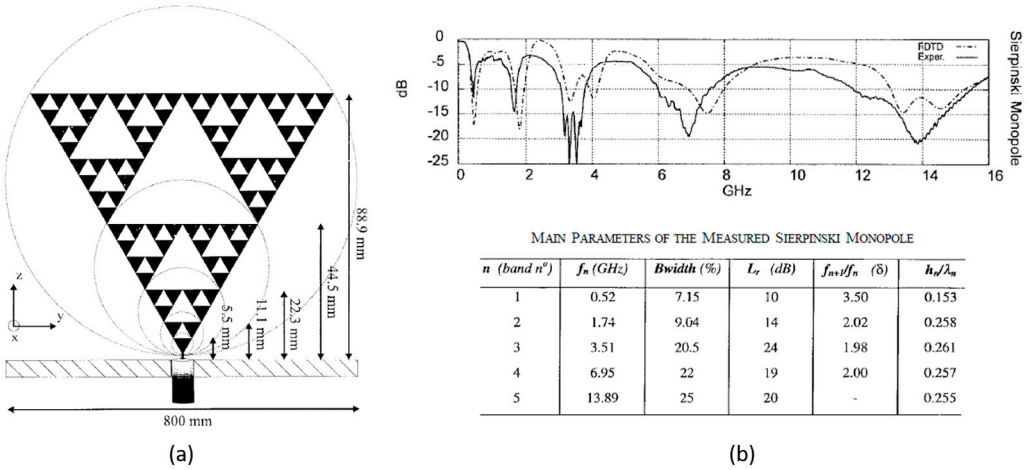

MAIN PARAMETERS OF THE MEASURED SIERPINSKI MONOPOLE

n (band n°)	f_n (GHz)	*Bwidth* (%)	L_r (dB)	f_{n+1}/f_n (δ)	h_n/λ_n
1	0.52	7.15	10	3.50	0.153
2	1.74	9.04	14	2.02	0.258
3	3.51	20.5	24	1.98	0.261
4	6.95	22	19	2.00	0.257
5	13.89	25	20	-	0.255

Figure 2. Penta-band Sierpinski monopole: (**a**) layout and sizes, (**b**) input reflection coefficient (Adapted with permission from [26], IEEE, 1998).

Figure 3a shows a small but long wire antenna based on the use of the Koch fractal curve. The antenna was presented in [27] with the aim to demonstrate how the space-filling properties of fractal shapes can be used to design small antennas. Actually, the reduction in the antenna size is an ultimate goal in a large number of applications, especially those involving mobile terminals. The Koch monopole, described in [27], is created by using the fractal construction method depicted in Figure 3a. The initial iteration, *K*0, is a straight monopole. The next iteration, *K*1, is obtained by applying similarity transformations to *K*0, including scaling by one third and rotations of 0°, 60°, −60°, and 0°, respectively. This process is repeated iteratively to obtain the subsequent elements *Ki* ($2 \leq i \leq 5$). Figure 3a shows the five-iteration version of the Koch monopole (i.e., *K*5), which has a height h equal to 6 cm, but a total length given by the formula $l = h \cdot (4/3)^5 = 25.3$ cm. In [26], five antennas have been implemented corresponding to the first five iterations of the Koch curve (see Figure 3a). Both experimental and numerical data have shown that the Koch fractal monopole can improve the performance of conventional monopoles (refer to Figure 3b). This demonstrates the possibility of using "miniaturized" fractal antennas that fit into smaller volumes while maintaining efficient performance.

Figure 4a shows a fractal antenna based on the Cantor set. The structure was proposed in [28] for designing a wideband antenna for energy harvesting applications. The unique property of fractal antennas to introduce multiple nearby resonances is exploited in [28] to provide wider bandwidths compared to conventional antennas. As illustrated in Figure 1a, the design of a Cantor fractal set is quite simple: the initial straight line is copied and divided into three equal segments, from which the central one is removed; the same procedure is then applied iteratively to the newly generated segments. In [28], the fractal iteration steps are repeated until an antenna bandwidth (BW) of 0.8–2.2 GHz is achieved

(i.e., 98% BW). Figure 4 shows a photo of the antenna prototype realized in [28] (Figure 4a) and its input reflection coefficient (Figure 4b).

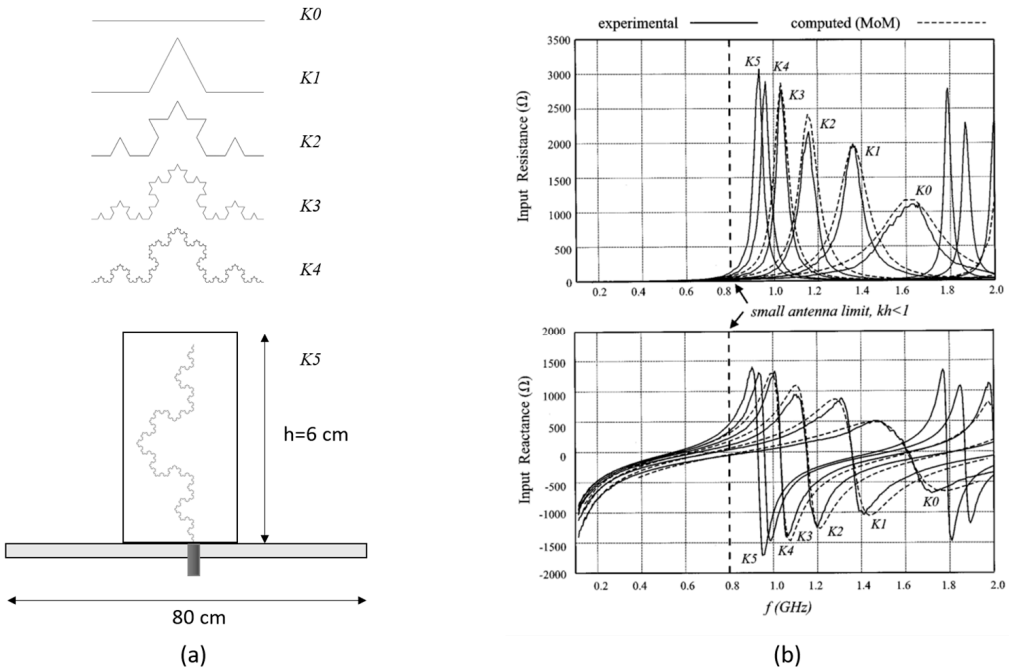

Figure 3. Five-iteration Koch monopole: (**a**) monopole layout construction, (**b**) input impedance (Adapted with permission from [27], IEEE, 2000).

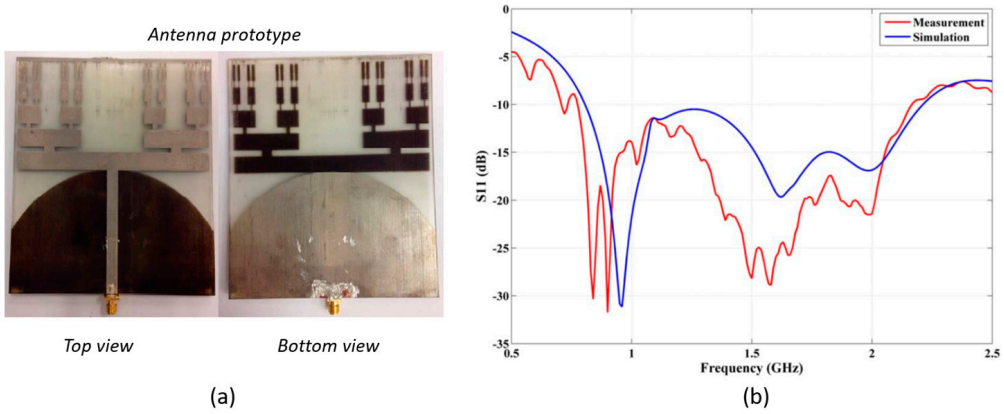

Figure 4. Cantor fractal antenna: (**a**) fabricated prototype, (**b**) input reflection coefficient (Adapted with permission from [28], EurAAP, 2017).

Figure 5 illustrates further examples of fractal antennas [29], including the Hilbert curve-based monopole, the Mandelbrot-based microstrip patch antenna, and the Koch island (or 'snowflake') fractal patch.

Several Hilbert monopoles were fabricated and tested in [30]. The length of the Hilbert monopole, given by the expression $L_n = \frac{4^{n+1}-1}{2^{n+1}-1}h$ (n = iteration number and h = height of the straight monopole—i.e., $n = 0$), increases with each iteration n, so that the resonant frequency decreases as n increases (Figure 5a). The results also showed that the antennas become electrically smaller as the fractal iteration increases at a higher rate compared to other fractal geometries.

A microstrip antenna with high directivity inspired by the Mandelbrot fractal (Figure 5b) was designed in [31]. The antenna was proposed as an alternative to antenna arrays in order to avoid the use of feed networks. However, the proposed solution does not offer

the possibility of pattern shaping or beam steering, making it particularly attractive in applications for which low-cost, low-weight and fixed-beam radiation patterns are required (e.g., small base station antennas used for WiFi, Industrial Scientific Medical (ISM) bands, the Internet of Things (IoT), etc.). Similarly, ref. [32] showed that a patch antenna with a fractal boundary, such as the Koch patch antenna depicted in Figure 5c, exhibits localized modes and behaves similarly to an antenna array, resulting in a microstrip patch antenna with high directivity. This technique has the advantage of increasing the directivity of a single element without the need for an array.

Finally, Figure 6 shows different fractal arrangements of array elements, including the Sierpinski carpet planar array, the Cantor ring array, the Cantor linear array, and the fractal tree. These arrangements are useful for producing thinned arrays and/or achieving multiband performance [8].

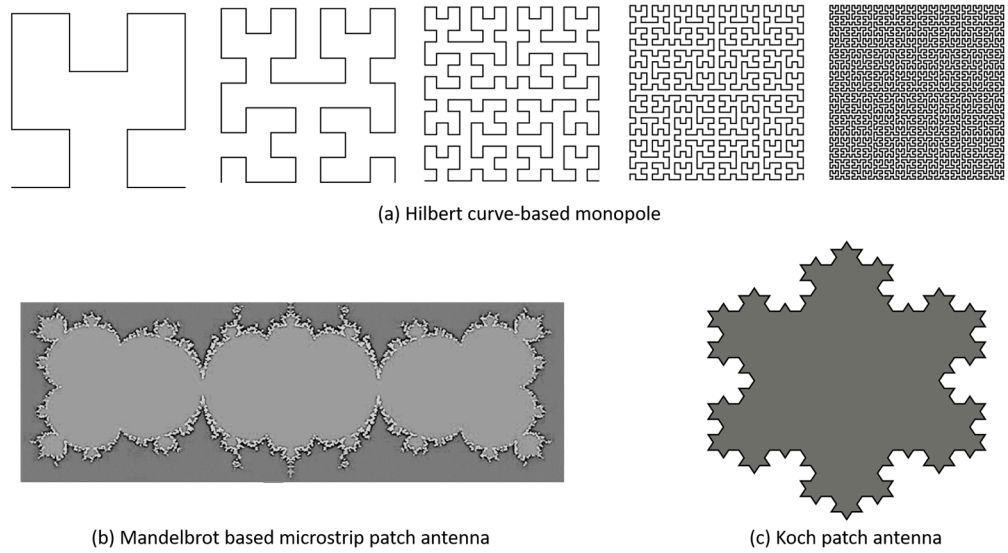

Figure 5. Various fractal antenna elements.

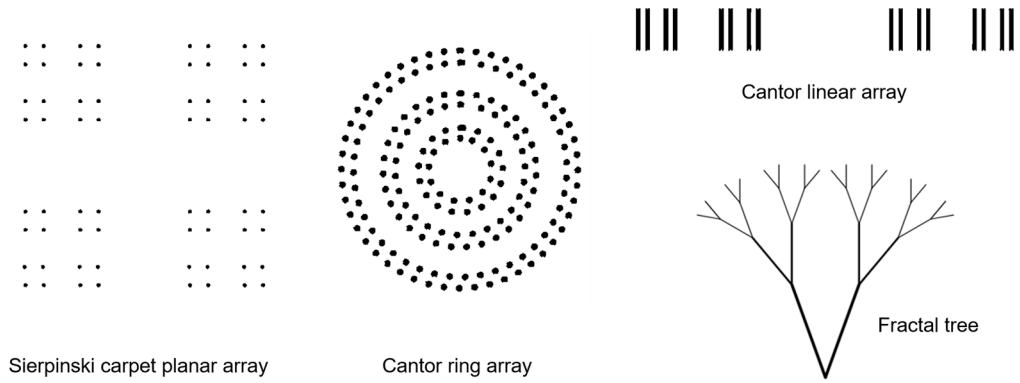

Figure 6. Various fractal array arrangements.

3. Fractal Reflectarray Antennas

Recently, several fractal antenna elements have been proposed for the design of reflectarray unit cells, which have a reduced size and quite good phase coverage [33]. Reflectarray antennas are flat reflectors made up of an array of microstrip elements illuminated by a feed antenna. Currently, the design of reflectarray antennas faces several challenges, such as the need to increase bandwidth, reduce losses, and miniaturize unit cells [34,35]. Tackling some of the above challenges, some fractal-based reflectarray configurations have been proposed in the literature. The miniaturization capabilities of fractal patches make them attractive for designing reflectarrays and phased-array antennas. Small array radiators offer many

advantages, including a reduction in mutual coupling and the ability to work with smaller array grids, which is useful to increase the bandwidth of reflectarray antennas [36,37] or to ensure good scanning performance over a wider frequency range.

3.1. Review of Existing Fractal Reflectarray Elements

Currently, the phase tuning mechanism of reflectarray antennas is realized by changing one or more geometrical/electrical parameters of the unit cell.

Various approaches have been presented in the literature, which can be essentially classified as follows [33–35,38–42]:

- variable-size patches, in which the reflection phase is controlled by varying the patch size around its resonant size;
- fixed-size patches, in which the phase-tuning mechanism is based on the use of a variable-length coupled element, such as a line and/or slot, embedded in the same cell;
- active patches loaded with reconfigurable devices or materials, such as varactors, PIN diodes, or liquid crystals [38–42].

The next subsections provide a brief review of the existing fractal reflectarray elements based on the first two approaches.

3.1.1. Variable-Size Fractal Patches

The first numerical analysis of a variable-dimension fractal reflectarray was performed in [43], in which some first-iteration fractal elements based on the Koch triangle, Koch square, and Minkowski shapes (Figure 7a) were proposed and studied. That analysis showed that all configurations had low losses (Figure 7c) but limited phase ranges (Figure 7b). According to the authors, the Minkowski element offers the widest phase range for a ±20% patch size variation around its resonance, despite a higher sensitivity to manufacturing errors (Figure 7b). However, the phase ranges provided by the configurations in Figure 7 may not be practical for a reflectarray design. To enhance this, one approach is to raise the percentage of patch variation, thereby reducing the benefits of fractal miniaturization.

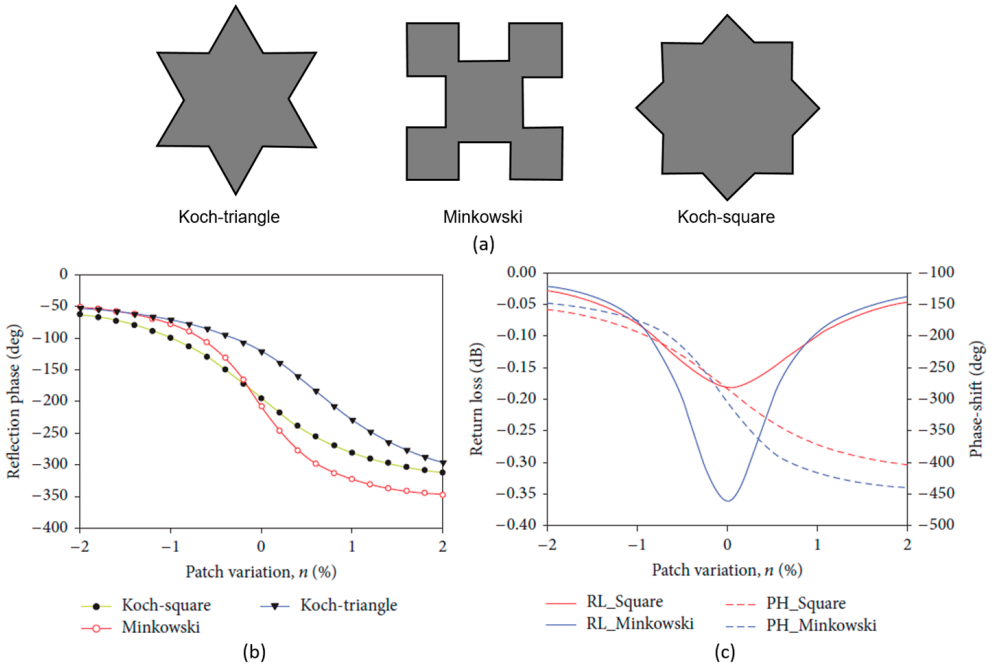

Figure 7. Simulated fractal unit cells @ f = 11GHz [33]: (**a**) variable-size fractal shapes, (**b**) reflection phase versus patch size variation percentage n% for different shapes; (**c**) reflection coefficient versus n% computed for Minkowski and square patches.

Additional examples of variable-sized fractal reflectarrays can be found in [44]. The goal of this work was to obtain a phase range exceeding 360 degrees, while also reducing the slope of the reflection-phase curve as a function of the element dimension. To this end, a novel fractal patch was proposed by introducing two vertical slots, symmetrically positioned with respect to the center of a square microstrip patch (Figure 8a). The dimensions of the slices, including their lengths, widths, and separations, are fixed independently, while ensuring that the overall structure fits within the square with sides of length L_1 [44]. The sliced square patch exhibits multiband behavior, resulting in a wide phase variation range at 10 GHz (Figure 8b). In [44], various parametric analyses were performed, involving cell size, substrate thickness, slot positions, and widths, in order to reduce the slope of the phase curve, which is critical for both the reflectarray bandwidth and the unit cell fabrication tolerances. Figure 8c demonstrates a good extension of the phase range and smaller curve slopes. However, this is achieved at the cost of an excessively large unit cell size (i.e., $0.7\lambda \times 0.7\lambda$ at 10 GHz), which prevents one from working with a small array lattice.

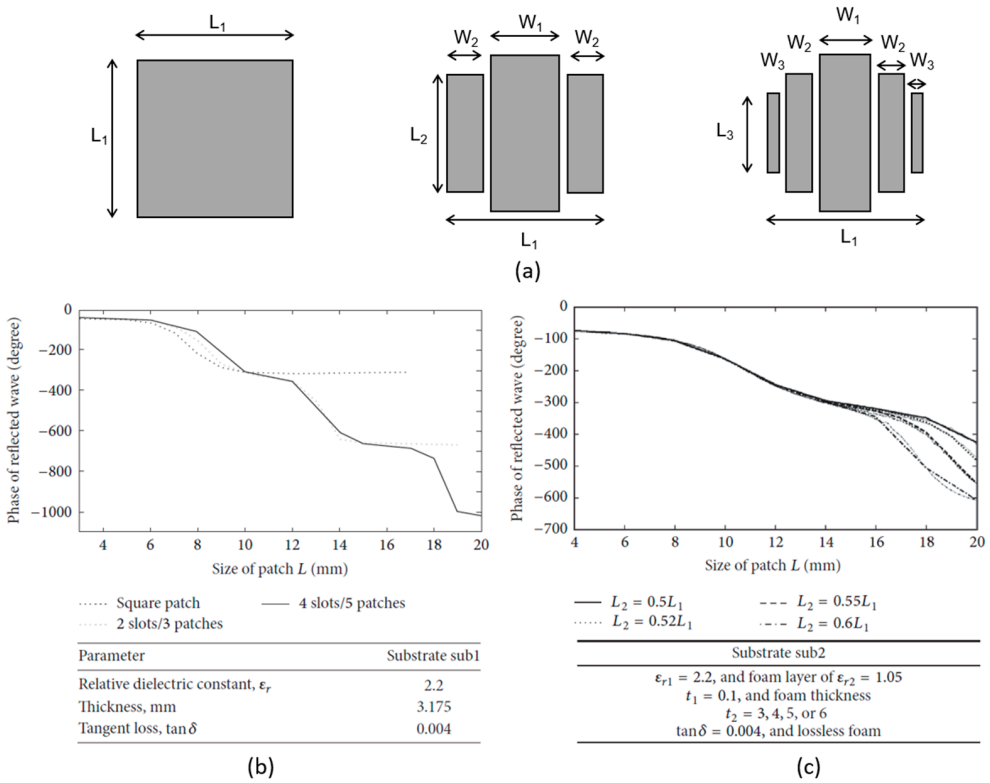

Figure 8. Multi-slice fractal patches [33]: (**a**) construction of the fractal element; (**b**) simulated reflection phase versus patch length of a fractal patch with two slots and four slots (@ f = 10 GHz); (**c**) linearized phase curves of two-slot multi-slice patch for different patch lengths.

3.1.2. Fixed-Size Fractal Patches

In [45], a new type of miniaturized reflectarray cell was introduced, which uses a fixed-size Minkowski patch. The phase tuning is obtained by using a variable-length slot, cut in the ground plane at the patch center (see Figure 9a). The fractal construction procedure is explained in Figure 9b. The initial element (i.e., n = 0) is a segment of length L_g called the "generator". In the first iteration (n = 1), the length of the generator is divided by three, then the central part is replaced by a rectangle with a base equal to $w(L_g/3)$, where w is the penetration factor varying between zero and one. The same procedure is applied iteratively to each side of the first-order fractal. The main advantage of this approach is related to the fixed size of the radiator, which allows one to exploit the miniaturization ability of fractals. Both the first- and the second-order Minkowski fractal patches were considered in [45]. The analysis showed that the resonant frequency of the cell decreases as

the slot length L_s increases (Figure 9c). Therefore, the fractal unit cell proposed in [45] can reduce the resonance frequency, resulting in a miniaturization effect. However, as a side effect, the slot in the ground plane produces unwanted back-radiations.

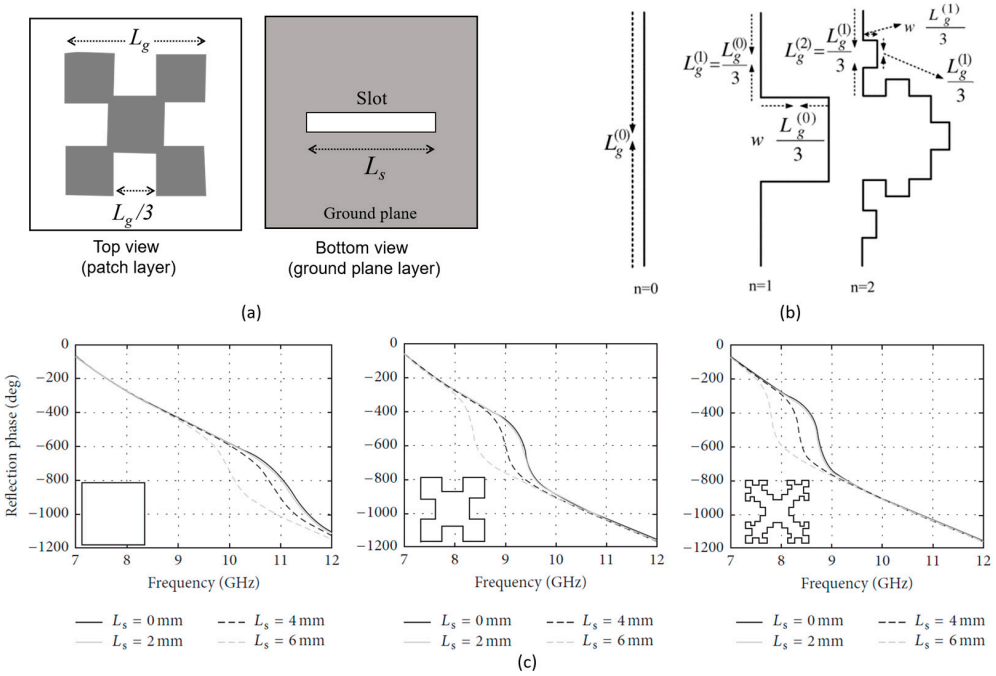

Figure 9. Minkowski patch with slotted ground plane: (**a**) unit cell, (**b**) fractal construction, (**c**) simulated reflection phase for square, first-, and second-order Minkowski patches (Adapted with permission from [45], IEEE, 2012).

A novel fixed-size Minkowski fractal patch was proposed in [46] for the design of small reflectarray elements. The inherent miniaturization capability of the fractal geometry is fully exploited in [46], leaving the patch length unchanged and using the fractal scaling factor to realize the phase tuning of the reflectarray cell. A square patch generator with the side length L is iteratively modified as described below (Figure 10a). In the initial iteration, a smaller square with a side length of SL is extracted from the center of each side of the generator patch. Here, S represents the fractal scaling factor, which varies from zero up to $L/3$. The fractal construction is reiterated by applying the above operation to each side of the first-order fractal structure, obtaining a more complex self-similar shape (Figure 10a). Since the resonant side length of the patch is equal to $L_n = (1 + 2S)^n L$ (n = iteration number, L_n = resonant length of n^{th} iteration patch), the cell can be miniaturized. To validate it, a fractal-shaped reflectarray element, embedded in a $0.3\lambda \times 0.3\lambda$ cell, was designed at 10 GHz to achieve a rather good phase agility of more than 300°. Ultimately, the fractal element proposed in [46] can offer, at the same time, good phase ranges, very small sizes (about 30% smaller than those of a standard variable-size reflectarray configuration), and lower reflection losses.

An alternative reflectarray unit cell was proposed in [47] (see Figure 11). Its layout is essentially derived from the first-iteration fixed-length Minkowski patch proposed in [46]. Figure 11c shows the patch geometry construction, which begins with a square element of dimensions L × L. Unlike the Minkowski patch, a smaller square of side SL is removed only from the center of the two lateral sides (i.e., the resonant sides, when a TE^x incident wave is assumed), resulting in a linearly polarized patch along the y-axis (see Figure 11a). The reflection-phase tuning is achieved by varying the fractal scaling factor S from 0 up to 0.45, leaving both the patch length and the distance between adjacent patches unchanged. In Figure 11b, it can be observed how the miniaturized reflectarray cells are able to offer good performance in terms of phase variation. Furthermore, as demonstrated in [47], they

exhibit uniform mutual coupling levels vs cell geometry variations, which is useful for wide-angle beam-steering applications.

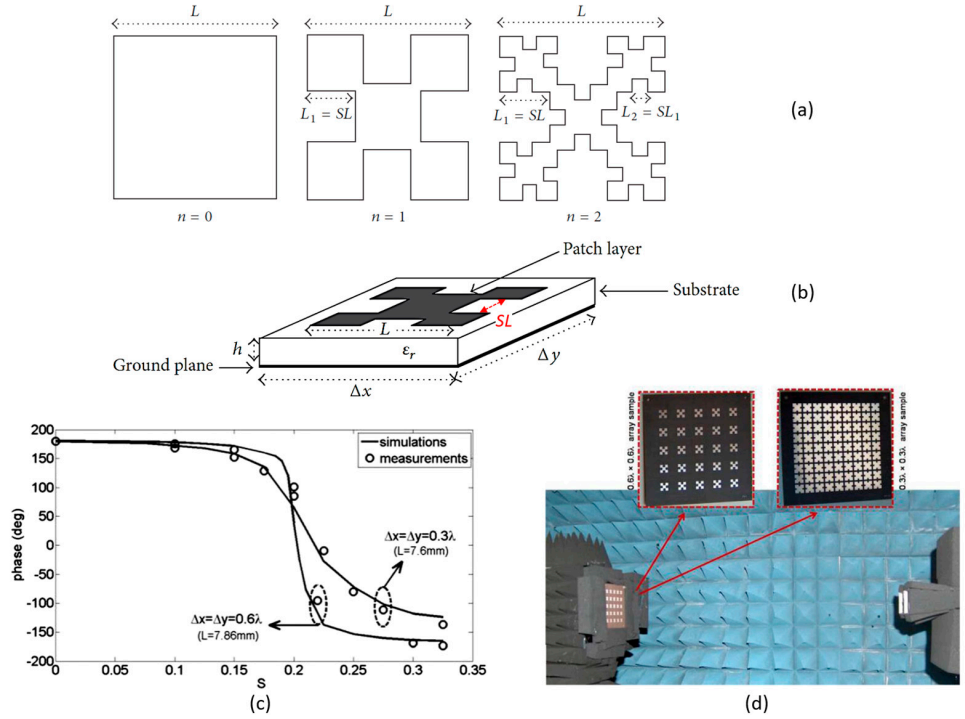

Figure 10. Minkowski patch with variable scaling factor S: (**a**) fractal construction; (**b**) unit cell geometry; (**c**) measured and simulated reflection-phase curves *vs* S at 10 GHz; (**d**) photo of the measurement setup with some fractal reflectarray samples (Adapted with permission from [46], IEEE, 2014).

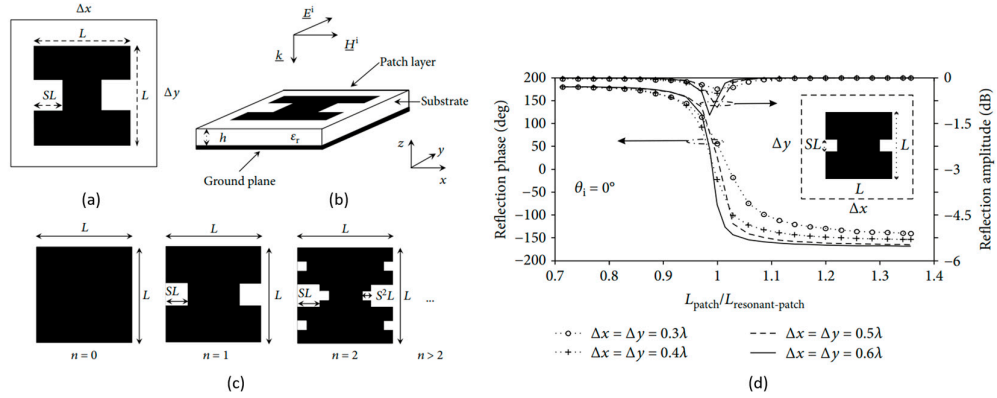

Figure 11. Miniaturized linearly polarized unit cell with a fractal patch with a variable scaling factor [47]: (**a**) top view, (**b**) 3D view, (**c**) fractal construction, (**d**) simulated reflection coefficient for different cell sizes.

In [48], a multilayer unit cell was proposed, consisting of a Minkowski fractal reflector with aperture-coupled phase stubs. The aim of the work was to extend the tuning phase range of Minkowski fractal reflectarrays. The authors achieved a linear phase curve with a range of more than two cycles and a return loss of less than 0.25 dB. However, this result was obtained at the cost of using a multilevel structure with a higher overall thickness.

3.2. Fractal Reflectarray Elements with Multifunctional Operation

Reflectarrays represent an interesting alternative in the development of innovative mmw antennas for future telecommunication systems (5G and 6G), being able to offer

high gains thanks to their spatial feeding mechanism [34,35]. Moreover, reflectarrays can provide several key skills, such as beam scanning, multi-beam or shaped radiation patterns, polarization diversity, and multi-frequency operations, which are useful for enhancing the capacity, coverage, and throughput performance of telecommunication systems. In order to achieve reflectarray unit cells with multifunctional operation, two fractal based cells have been proposed in [49,50], respectively, for dual-band applications at 28/38 GHz and for dual-band/dual-polarization operation within the Ka band (i.e., 27 and 32 GHz). Thanks to their compact and versatile nature in achieving frequency and/or polarization diversity, both unit cells have been proposed for 5G applications.

In particular, the dual-band unit cell proposed in [49] is composed of two pairs of alternately arranged fractal patches (Figure 12a), each designed to operate around a specific resonant frequency (i.e., f_1 and f_2). The single patch layout is based on the first iteration of the fixed-length Minkowski patch originally proposed by the authors in [46]. The patch geometry shown in Figure 12a is characterized by an initial square element of side length L_n (n = 1, 2). A smaller $S_nL_n \times S_nL_n$ square ($0 < S_n < 0.45$) is cut from the center of the two lateral sides (i.e., the resonant sides), resulting in a linearly polarized element along the y-axis (Figure 12a). The reflection-phase tuning is achieved by independently varying the scaling factor S_n of each element while keeping the patch dimension as $L_n \times L_n$.

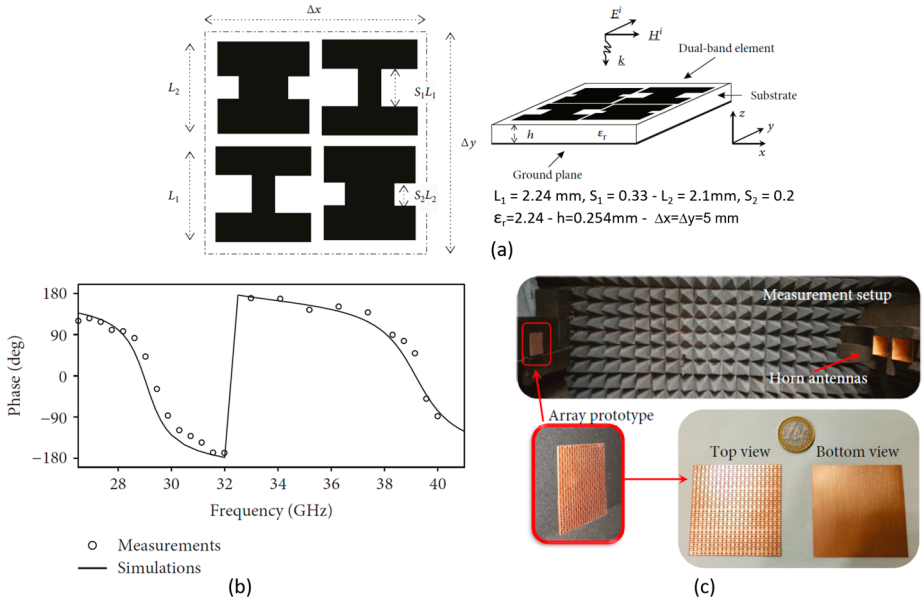

Figure 12. Dual-band fractal unit cell [49]: (**a**) top view and 3D view; (**b**) measured and simulated reflection phase; (**c**) measurement setup and reflectarray prototype.

As shown in [49], this configuration allows for minimal inter-element spacing and negligible mutual coupling effects between the two frequency bands. This guarantees an independent phase-tuning mechanism for both desired bands. A reflectarray consisting of 11 × 11 identical cells (Figure 12c) was printed on a 0.254 mm thick DiClad880 substrate as experimentally validated in [49]. The cell reflection-phase curve was measured in the frequency range from 26.5 to 40 GHz, achieving a phase variation of approximately 300° around both operating frequencies. The simulations and measurements were in good agreement (Figure 12b), validating the dual-band fractal cell.

A similar concept was applied in [50] to design a single-layer dual-band/dual-polarized reflectarray cell. The proposed unit cell, as described in [50], comprises four miniaturized fractal-based elements (Figure 13a). The patches are arranged in two pairs, each operating at two different frequencies within the Ka band (i.e., 27 and 32 GHz). Each pair comprises two linearly polarized patches rotated by 90° to provide double polarization operations at both frequencies. The scaling factor of each element was independently varied to adjust

the reflection phase for each frequency/polarization. As shown in [50], the reflectarray cell offers several advantages, including a simpler and thinner structure and smaller unit cell sizes at both operating frequencies (0.49λ at 27 GHz and 0.58λ at 32 GHz), which preserves the ability to direct the main beam at wide scan angles. In [50], the full-phase variation was measured for both polarizations at both operating frequencies (Figure 13b). Additionally, a dual-band/dual-polarized prototype was designed and tested, demonstrating the unit cell's flexibility in providing arbitrary beam directions/shapes at each frequency for both polarizations (see Figure 13c).

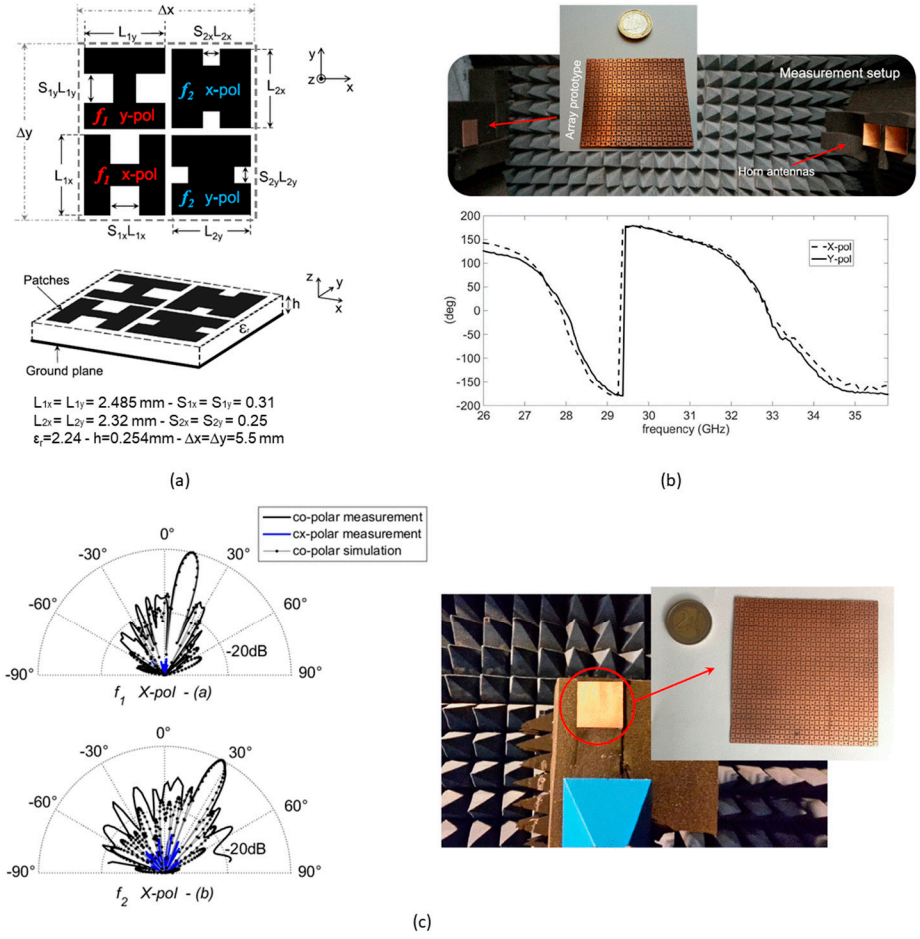

Figure 13. Dual-band/dual-polarized unit cell [50]: (**a**) top view and 3D view; (**b**) reflection-phase measurement setup and measured phase curves for different polarizations; (**c**) measured and simulated radiation patterns for X-polarization at f_1 = 28.7 GHz and f_2 = 32.8 GHz, and prototype photo.

4. Fractal Metasurfaces

Metasurfaces are two-dimensional structures composed of subwavelength unit cells arranged in a precise pattern. These structures are engineered to manipulate and control the propagation of electromagnetic waves. Metasurfaces offer unique properties and functionalities not found in traditional surfaces or bulk materials. The design of metasurfaces involves tailoring the shape, size, and arrangement of the subwavelength elements to achieve wavefront manipulation. By controlling the interaction between the incident electromagnetic waves and the metasurface, various effects can be achieved, including focusing, polarization conversion, beam steering, and absorption. This versatility makes them useful in various applications, such as wireless communications, electromagnetic compatibility, cloaking, energy harvesting, sensing, and beyond. However, metasurfaces also exhibit a number of limitations, such as the following:

- sensitivity to the impinging wave incident angle which may lead to performance degradation or altered functionalities;
- fabrication challenges related to the precision and the costs of the adopted manufacturing process in realizing subwavelength elements.

In the last decade, fractal metasurfaces have been proposed and studied as an exciting alternative to traditional electromagnetic metasurfaces [10,51–59]. In fact, the autosimilarity and miniaturization capabilities of fractals not only allow for the realization of very compact devices, but can enable technologies for multiband and broadband applications. Moreover, fractal metasurfaces have been of interest in various industrial applications such as radiation transfer, power control, antenna gain enhancement, and cloaking systems, resulting in several patents [51,52].

Below are examples of fractal metasurfaces designed for various frequency bands and applications. Specifically, this section is divided into subsections that examine the following: fractal metamaterial absorbers, including a brief study of how fractal shapes can affect absorber performance; fractal metamaterial polarizers; and metamaterial surfaces for antenna applications. This section concludes by outlining the current challenges of and potential future developments for fractal metasurfaces.

4.1. Fractal Metamaterial Absorbers

One important application of metasurfaces is in electromagnetic wave absorption. Metamaterial absorbers (MAs), as proposed in [60], can be designed to efficiently absorb a specific frequency. These can be used across the frequency spectrum from RF to ultraviolet (UV) for various applications [61–64], including the reduction in electromagnetic interference, the mitigation of multipath problems in indoor wireless applications, 5G communications, the improvement of the electromagnetic compatibility of electronic devices, and the design of photonic devices.

MAs typically consist of a periodic frequency-selective surface printed on a thin, grounded dielectric substrate (see Figure 14a). Some examples of unit cell geometries are reported in Figure 14b. To achieve the absorption of a specific frequency, f_0, it is necessary to synthesize the MA unit cell to match the impedance of free space, ξ_0. In this way, the unit cell reflection coefficient, $\Gamma = \frac{Z_{cell}-\xi_0}{Z_{cell}+\xi_0}$, approaches zero, obtaining a near-unity absorption ($A=1-|\Gamma|^2 \rightarrow 1$). Several MA unit cells have been proposed in the literature [62] in the last few decades. More recently, the fractal concept has been used to create compact and multiband metamaterial absorbers. Although the results obtained from the application of fractals are very interesting, this approach is still considered to be in the development phase. Therefore, ongoing research in these areas continues to explore new designs.

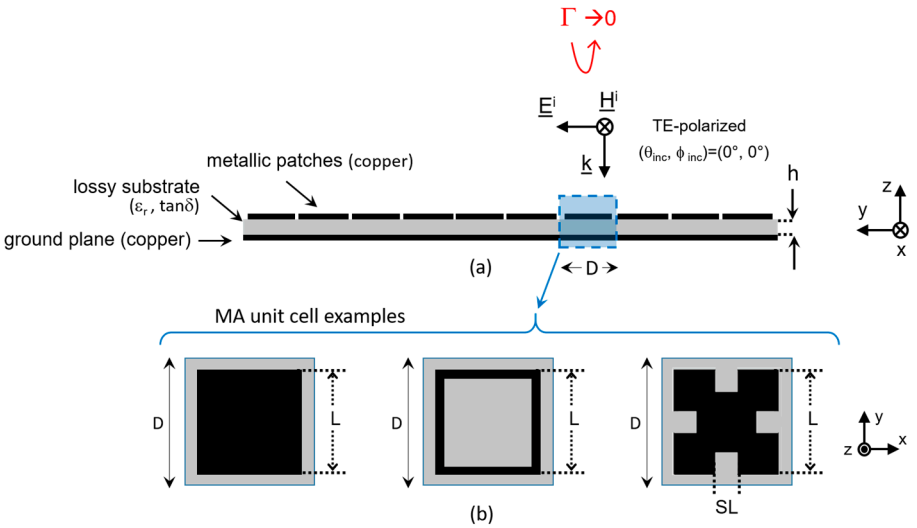

Figure 14. General structure of a metamaterial absorber: (**a**) side view; (**b**) examples of unit cells.

4.1.1. Impact of Fractals on the Electromagnetic Performance of Metamaterial Absorbers

In this subsection, the Minkowski fractal is used as an example to illustrate the impact of fractal shapes on the electromagnetic performance of metamaterial absorbers. Figure 15a displays the schematic of square, first-iteration Minkowski and second-iteration Minkowski fractal cells that are designed to operate in the UHF frequency band. Specifically, the square patch (n = 0) is designed for absorption at 880 MHz (Figure 15). Subsequently, the first (n = 1) and second (n = 2) fractal cells are constructed by considering two distinct cases in parallel, namely the cell with scaling factor S = 0.2 (Figure 15b) and the cell with scaling factor S = 0.25 (Figure 15c). The simulated absorption coefficients for both cases are shown in Figures 15b and 15c, respectively. It can be clearly seen that the main effect of the fractal cells is the reduction in the resonance frequency. As the order of the fractal geometry increases, the resonant frequency decreases compared to the square patch for all considered scaling factors S. Furthermore, the rate of frequency reduction increases as S increases. Thus the use of fractal geometries in microstrip element design enables a greater electrical length to be packed into a smaller area. In particular, the first and second Minkowski cells exhibit reductions of 14.3% and 21.4%, respectively, compared to the standard square patch when S = 0.2. Meanwhile, for S = 0.25, the percentage reductions are 35.7% and 40.7%, respectively. It is important to note that the first iteration of Minkowski is responsible for most of the size reduction.The justification for the aforementioned behaviour is described in Section 3.1.2 for Minkowski-based reflectarray cells. In this case, the resonant length of the n^{th} iterated patch is estimated to be $L_n = (1 + 2S)^n L$, where n represents the number of iterations. The formula demonstrates that the electrical length of the fractal patch increases with both n and S, resulting in a lower resonant frequency. Therefore, to achieve resonance at the desired working frequency, the fractal element must be miniaturized.

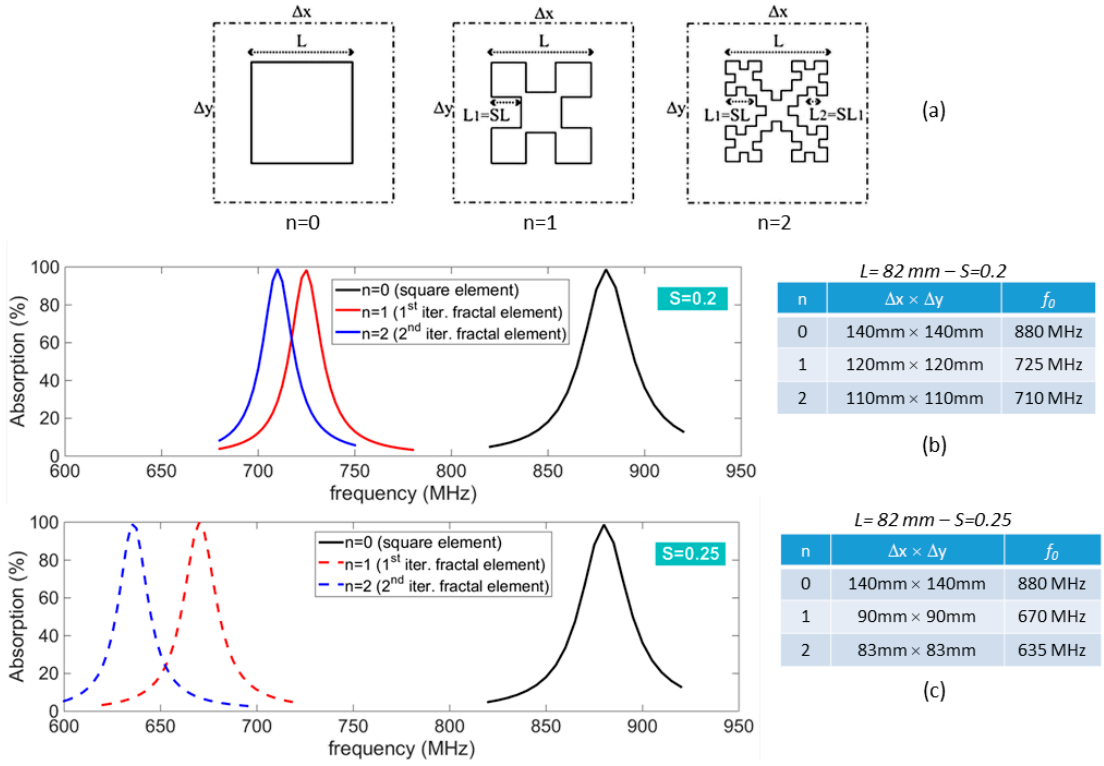

n	Δx × Δy	f_0
0	140mm × 140mm	880 MHz
1	120mm × 120mm	725 MHz
2	110mm × 110mm	710 MHz

n	Δx × Δy	f_0
0	140mm × 140mm	880 MHz
1	90mm × 90mm	670 MHz
2	83mm × 83mm	635 MHz

Figure 15. Simulated absorption of fractal-based MAs: (**a**) fractal unit cells; (**b**) unit cell size and absorption coefficient for S = 0.2; (**c**) unit cell size and absorption coefficient for S = 0.25.

Thanks to their miniaturization capabilities, fractals have become widely used for designing compact and easily integrable microwave absorber structures. Furthermore, as discussed in the following sections, the self-similarity and compactness of fractal geometries

allow for the implementation of multiband and broadband absorbers, thus saving space compared to conventional metamaterial absorbers.

4.1.2. Examples of Fractal-Based MAs

The Minkowski fractal geometry proposed in [53,54] can be used to create small absorber cells that are suitable for mitigating multipath phenomena in the European RFID UHF band. The compact size of fractal geometries has been exploited to design a dual-band microwave absorber operating in the UHF band [54]. The MA unit cell, shown in Figure 16a, consists of two pairs of Minkowski patches arranged alternately. The fractal elements in the pairs were synthesized to operate at specific resonant frequencies, namely 878 MHz and 956 MHz, resulting in absorption peaks greater than 99%. An absorber plate measuring 125 mm × 125 mm and composed of 18 × 18 fractal elements was prototyped and experimentally validated (see Figure 16b). The configuration achieved perfect absorption in the dual-frequency operating mode, despite being thinner and smaller than standard microwave absorber configurations [54]. Furthermore, the panel exhibited stable angular behavior (see Figure 16b).

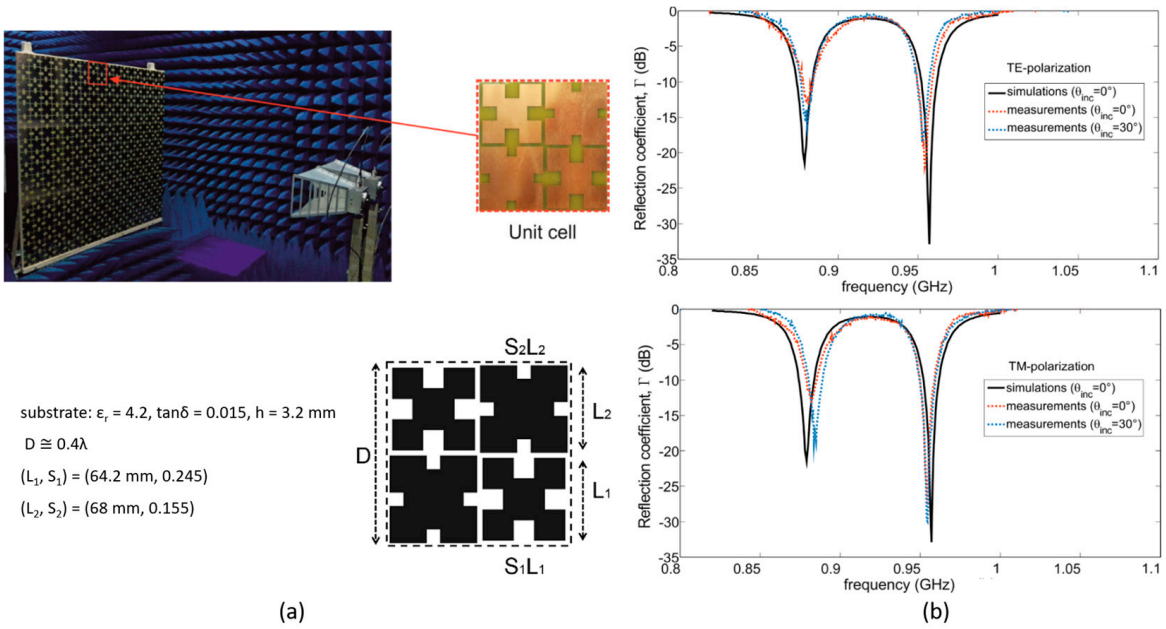

Figure 16. UHF fractal MA unit cell [54]: (**a**) cell layout and free-space measurement setup with the particulars of the fabricated MA absorber, (**b**) comparison between measured and simulated reflection coefficients.

Another example of fractal MAs is the polarization-independent metamaterial energy harvester (EH) proposed in [55]. Metamaterial structures are a promising alternative to conventional rectennas for RF energy harvesting systems. They offer significant advantages in terms of increased harvested power and a greater efficiency in the initial RF-to-AC power conversion stage [65–69]. Figure 17a shows a metamaterial cell consisting of a miniaturized Minkowski fractal element printed on a thin grounded dielectric layer. The cell is loaded with two resistive loads that model the rectification circuitry. The unit cell analyzed in [55] provides high absorption rates, good angular stability, and high polarization independence in the 2.45 GHz Wi-Fi frequency band. In addition, a 9 × 9 metamaterial EH was designed and simulated, demonstrating a high RF-to-AC efficiency of 96.5% (see Figure 16b). Moreover, the finite-size harvester exhibits polarization-insensitive behaviour, making it highly attractive for the development of eco-friendly energy-harvesting solutions.

In [56], a circular fractal structure was proposed to design a tri-band polarization-insensitive metamaterial absorber for stealth technology. The MA was printed on an FR4 dielectric substrate and backed by a metallic layer. The proposed fractal construction process starts with an initiator circle (iteration 0). Next, four small circles, tangent to each other, are inserted into the initiator (Figure 18a). This shape represents the first iteration of the fractal geometry and is called the generator. As shown in Figure 18a, the subsequent iterations are generated by repeating the process described above. In particular, in [56], the construction process was stopped at iteration 2 to design the MA cell shown in Figure 18b, resulting in the measured absorption coefficient in Figure 18c.

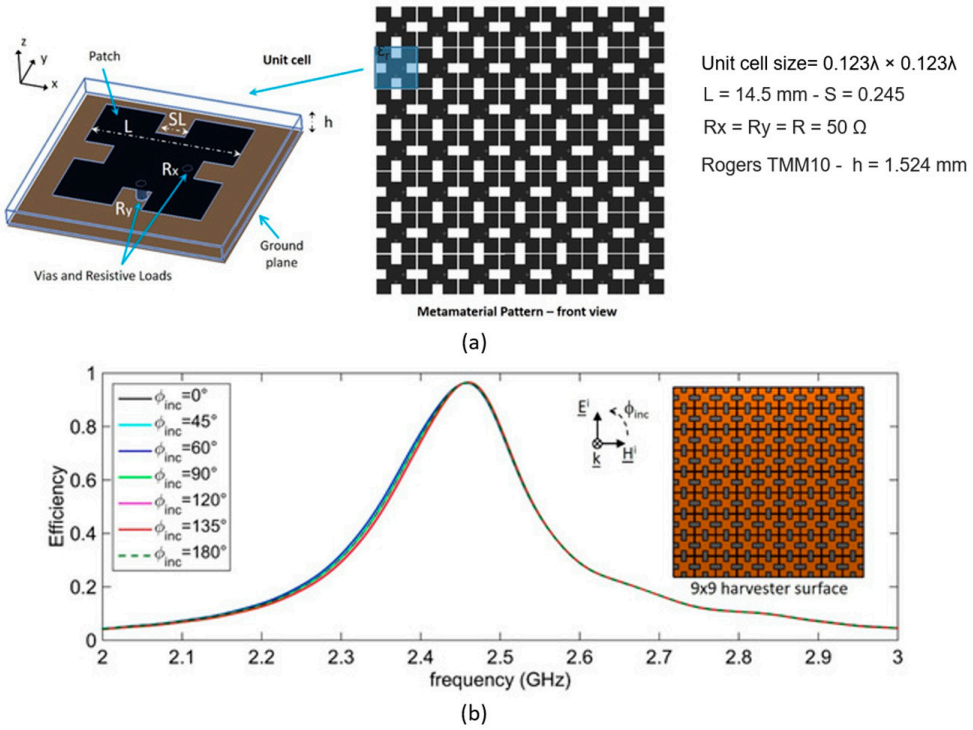

Figure 17. Minkowski MA unit cell for ambient power harvesting [55]: (**a**) top view and 3D view, (**b**) RF-to-AC efficiency of a 9 × 9 harvester for different polarization angles ϕ_{inc} at normal incidence.

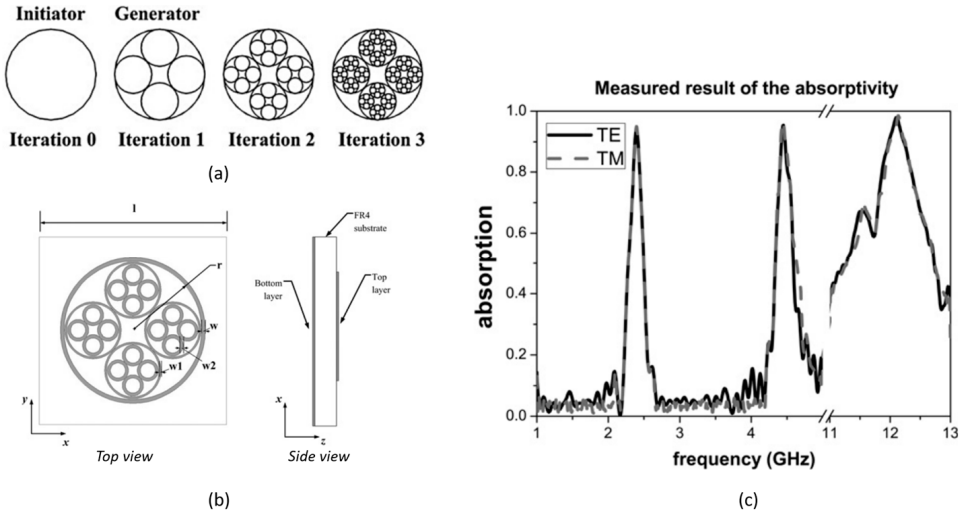

Figure 18. Circular fractal-based MA: (**a**) fractal construction, (**b**) circular fractal MA unit cell, (**c**) measured absorption coefficient (Adapted with permission from [56], IET, 2016).

Reference [57] proposes a fractal-based metamaterial structure with lumped resistors, using a combination of the Sierpinski curve and Minkowski fractal (see Figure 19). The structure is printed on a 1.6 mm thick FR4 substrate with an air gap of 12.5 mm. This geometry enables the design of a perfect tri-wideband metamaterial absorber that covers the frequency bands of 1.7 to 2.6 GHz, 4.56 to 5.59 GHz, and 12.37 to 13.29 GHz (Figure 18c), at the expense of a thick structure.

In reference [58], a Minkowski inspired circular fractal metamaterial microwave absorber was proposed for multiband applications. The absorber structure consists of a novel geometry of second-order circular fractal rings printed on a grounded FR4 dielectric substrate. The fractal patch is achieved using a circular ring, called the initiator (see $n = 0$ in Figure 20a), followed by a level 1 fractal ($n = 1$), which is then extended to an upper iterated fractal ($n = 2$). Figure 20b shows the absorptivity of the initiator and generator structures, as well as the proposed Minkowski-inspired circular fractal absorber (denoted by $n = 0$, 1, and 2, respectively). The Minkowski-inspired circular fractal MA ($n = 2$) exhibits a greater number of absorption peaks compared to the initiator ($n = 0$) and the generator absorber ($n = 1$). More specifically, it offers four absorption peaks at 5.6, 11.5, 15.4, and 17.6 GHz with absorptivities greater than 90%, and two peaks at 1.8 and 8.4 GHz with absorptivities greater than 80%.

In [59], a triple-band metamaterial absorber was proposed for applications requiring very high compactness values. Unlike previous multiband absorbers, this implementation incorporates fractal geometry into an artificial transmission line framework (Figure 21b). The resulting large inductive-capacitive values make the element compact, approaching $\lambda_0/15$ at the lowest fundamental resonant frequency. The absorber exploits the self-similarity and space-filling capabilities of fractals. The fractal perturbed element is significantly smaller due to the engineered semi-lumped circuit elements and therefore exhibits multifunctional self-resonant properties. Figure 21a shows the simulated results of the MA, displaying three distinct absorption peaks.

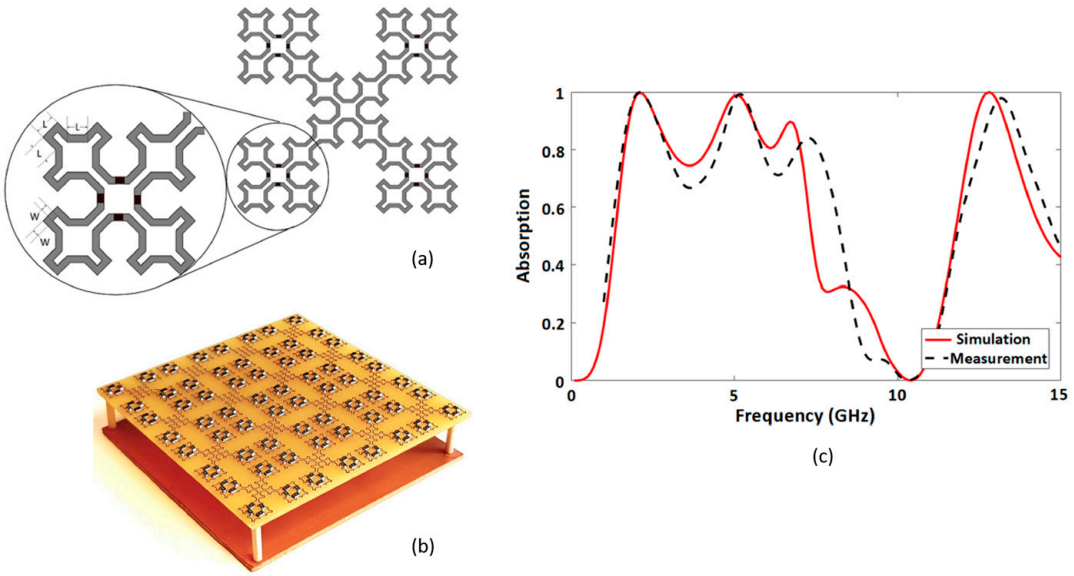

Figure 19. Sierpinski–Minkowski fractal MA: (**a**) unit cell structure, (**b**) fabricated absorber, (**c**) measured absorption coefficient (Adapted with permission from [57], IET, 2019).

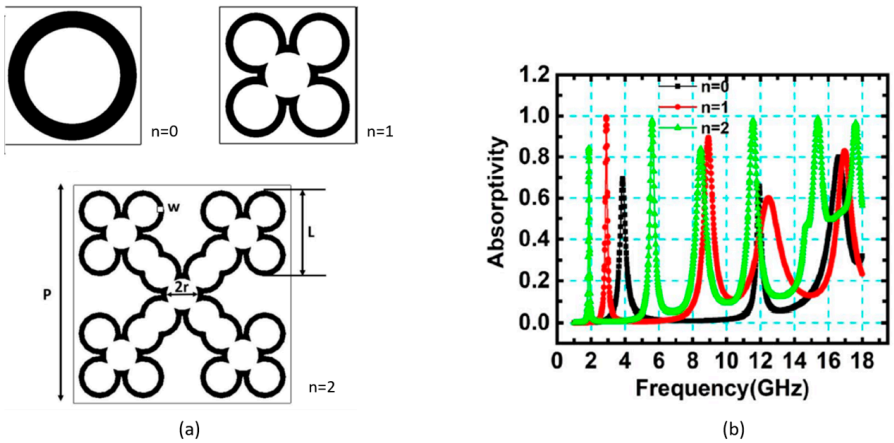

Figure 20. Minkowski-inspired circular fractal MA: (**a**) fractal construction, (**b**) simulated absorptivity (Adapted with permission from [58], Springer Nature, 2023).

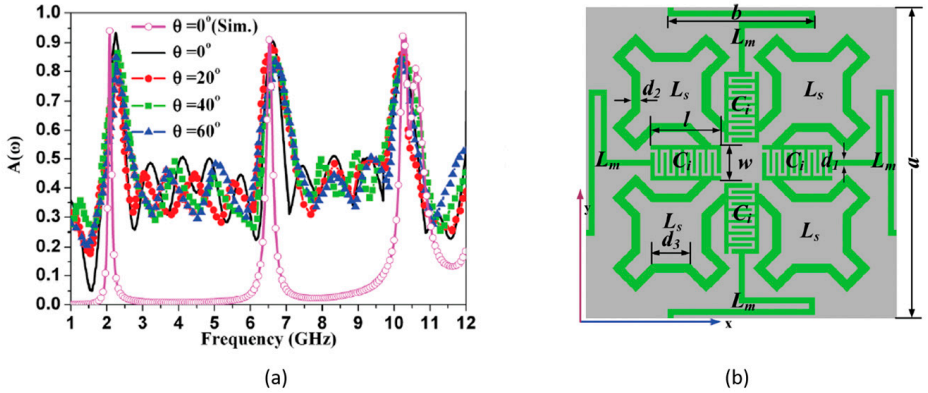

Figure 21. Triple-band metamaterial TL absorber MA [59]: (**a**) measured absorption as a function of frequency at different angles of incidence; (**b**) top view of the MA element. (Reproduced with the permission from He-Xiu Xu, Physical Review B; published by American Physical Society, 2012).

4.2. Fractal Metamaterial Polarizers

Metamaterials are often used in the design of polarizers to manipulate the polarization state of electromagnetic waves [70]. A polarizer is a device that selectively transmits or absorbs EM waves based on their polarization. Metamaterials can be designed to manipulate the polarization of electromagnetic waves in novel ways. This includes controlling the orientation or ellipticity and even switching between different polarization states. Such capabilities are valuable in applications ranging from telecommunications to imaging. Traditional polarizers can be limited in their ability to operate over a wide range of frequencies. Metamaterial-based polarizers can be designed to provide broadband capabilities, allowing for effective polarization control over a wide frequency range [70]. In addition, metamaterials provide a platform for designing multifunctional polarizers that can perform additional functions beyond polarization control. For example, they can be integrated into devices that combine polarizing capabilities with filtering or beam-steering functions. Metamaterial-based polarizers have applications in antennas, imaging systems, and optical devices [70]. They can be integrated into these systems to increase performance, improve signal quality, or enable new functionalities.

Recently, some fractal-based metamaterial polarizers have been proposed in the literature. In particular, a compact dual-band circular polarizer using a twisted Hilbert chiral metamaterial was proposed in [71]. The paper demonstrated how chiral behavior is enhanced by fractal perturbation. The layout of the proposed meta-atom is shown in Figure 22. The structure can emit circularly polarized waves from a linearly polarized

incident wave with high transformation coefficients over two microwave bands. In ref. [72], a fractal-based metasurface was investigated as a dual-polarization converter operating in the terahertz (THz) band. Figure 22b shows the layout of the structure, for which the top metasurface is patterned as an array of H-shaped tree-like fractal resonators. The converter has been numerically tested, demonstrating its ability to perform both linear-to-cross (LX) and linear-to-circular (LC) polarization conversions over three operating bands, namely 1.2–1.83 THz, 2.52–3.1 THz, and 3.78–3.9 THz.

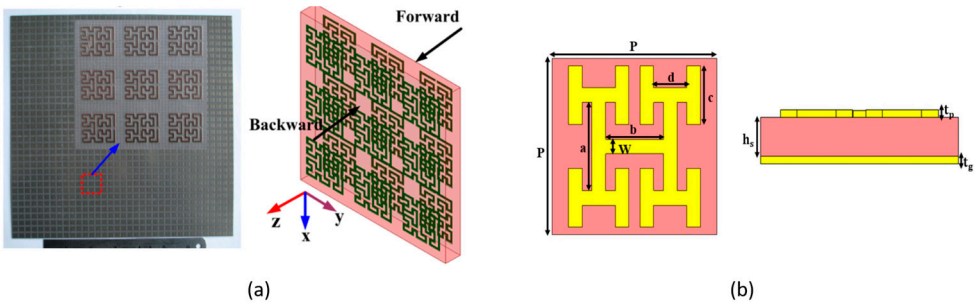

Figure 22. Metamaterial fractal polarizers: (**a**) dual-band circular polarizer using a twisted Hilbert chiral metamaterial [71], (**b**) H-shaped tree-like fractal metamaterial polarizer [72].

4.3. Fractal Metamaterial in Antenna Applications

Over the last two decades, metamaterials have become increasingly popular in the antenna community due to their ability to improve the performance of antenna systems. They offer advantages such as bandwidth enhancement, gain improvement, miniaturization, stealth capabilities, and reductions in mutual coupling [73–80]. Combining fractal metamaterials with antennas is an innovative approach in EM technology. Actually, fractal metamaterials have unique properties (e.g., miniaturization) that can improve the functionality of antennas. Below are some examples of antennas that use fractal metamaterials [81–85].

In [81], a compact single-feed circularly polarized (CP) patch antenna was proposed and investigated based on the combined use of meta-surfaces and meta-resonators for gain enhancement (see Figure 23a). A complementary crossbar fractal tree slot was used as a meta-resonator to enable the antenna to radiate circularly polarized (CP) waves in single-band or dual-band operation and to facilitate further miniaturization.

A novel miniaturized CP microstrip antenna operating in the UHF band (920–925 MHz) was designed in [82]. The antenna miniaturization was achieved by a special cross-shaped fractal metamaterial structure inserted between the patch and the ground plane (see Figure 23b).

In [83], a strategy was proposed to reduce the cross-polarization (XP) radiation of a microstrip antenna by using the fractal-perturbed mushroom structure shown in Figure 23c. This method achieved XP suppression over several operating bands (1.5 GHz, 2.96 GHz, and 7.7 GHz) without compromising the co-polarization patterns, such as the antenna gain and directivity.

Hilbert-shaped magnetic waveguide metamaterials to reduce the electromagnetic coupling of microstrip antenna arrays were proposed and developed in [84], showing a high decoupling efficiency (Figure 23d).

Recently, metamaterials have also been used to fabricate lenses for microwave applications, including beam shaping, beam steering, and imaging. The literature presents bulk lenses made of 3D metamaterials or planar lenses made of metasurfaces [86–90]. Several interesting configurations using fractal meta-elements for lens antennas have also been presented [88–90]. In addition, in 2018, Fractal Antenna Systems Inc. was granted a US patent for a planar lens that uses fractal metamaterials to bend electromagnetic waves [91]. In [88], a left-handed fractal material-based three-dimensional superlens was proposed for C-band operation using second-order iteration Sierpinski fractal curves. In [89], a broadband three-dimensional (3D) emission system was proposed for beam-shaping and

beam-steering applications. The system comprises an omnidirectional source antenna and multiple lenses with a 3D gradient index of refraction (GRIN). The lenses are based on a Sierpinski fractal ring meta-element, as shown in Figure 23e. The same fractal metamaterial element was used in [90] to design an octave bandwidth half-Maxwell fish-eye (HMFE) lens antenna for C-band operation.

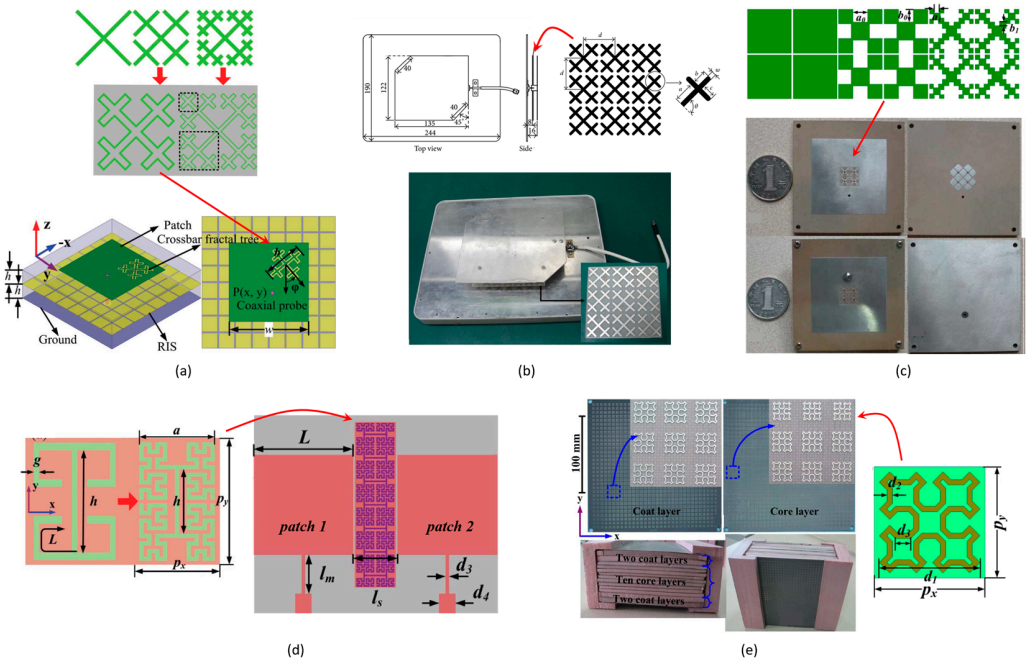

Figure 23. Fractal metamaterials integrated antennas: (**a**) compact single-feed CP patch antenna based on the combined use of meta-surfaces and meta-resonators (Adapted with permission from [81], IEEE, 2013), (**b**) miniaturized CP microstrip antenna loaded by cross-shaped fractal metamaterial surface [82], (**c**) microstrip antenna integrated with fractal-perturbed mushroom structure (Adapted with permission from [83], IEEE, 2014) (**d**) fractal metamaterial for mutual coupling reduction in microstrip antenna array [84], (**e**) fabricated GRIN slab lens and fractal meta-element (Adapted with permission from [89], Springer Nature, 2014).

4.4. Future Developments of Fractal Metasurfaces

As previously discussed, fractal metasurfaces have demonstrated significant potential in various fields, including telecommunications, EMI reduction, energy harvesting, and cloaking devices. However, further exploration is required in these areas, as well as expansion into new areas such as wearable devices and biosensors [92–95]. Future developments of fractal metamaterials should consider various aspects, including challenges, technological advancements, and potential applications. To tackle the manufacturing challenges associated with the precision and cost of subwavelength fractal elements, it is crucial to concentrate on advancements in fabrication techniques that allow for the creation of intricate and precise fractal structures at smaller scales. Techniques like 3D printing and nanolithography may be essential in achieving finer details and more complex fractal geometries. Additionally, the ability to customize and adjust the properties of fractal metamaterials by incorporating materials or components with adjustable parameters is a crucial aspect. In the future, fractal metasurfaces may become increasingly multifunctional, offering a wider range of capabilities in a single device. The trend towards miniaturization is expected to continue, with fractal metasurfaces finding applications in smaller devices and systems. It is possible that integration with existing technologies, such as consumer electronics, medical devices, and wearable technology, will become more prevalent.

In conclusion, the future development of fractal metamaterials is promising, driven by ongoing advances in fabrication techniques, expanding applications, and integration with other cutting-edge technologies.

5. Conclusions

The concept of fractals as applied to antennas and metasurfaces has been discussed in this paper. A comprehensive review of fractal antennas and metasurfaces has been undertaken, exploring their design principles and performance. Several examples of fractal-based antennas and metasurfaces have been discussed and compared, highlighting their advantages, limitations, and potential applications. Some multifunctional fractal reflectarrays have been presented, offering polarization and frequency diversity, which are useful for enhancing the capacity, coverage, and throughput performance of new generation telecommunication systems. Additionally, the potential of fractal metasurfaces has been discussed, demonstrating their application in UHF-RFID multipath mitigation and energy harvesting systems.

In conclusion, the application of fractal concepts to antenna and metasurface design has brought significant advancements and advantages in the field of electromagnetics. Fractal antennas and metamaterials, with their self-similar and intricate geometric patterns, offer several benefits over traditional structures, such as their multiband/wideband operation, compact size, and high degree of design flexibility. Ongoing research and development in these areas aim to explore new designs and fabrication techniques to further advance their capabilities and broaden their range of applications, such as for statistical arrays [96,97].

Author Contributions: Conceptualization, F.V. and S.C.; methodology, F.V.; validation, F.V., S.C. and A.B.; investigation, F.V. and S.C.; resources, F.V.; writing—original draft preparation, F.V.; writing—review and editing, F.V. and S.C. All authors have read and agreed to the published version of the manuscript.

Funding: This research was funded in part by the European Union under the Italian National Recovery and Resilience Plan (NRRP) of NextGenerationEU, in partnership with "Telecommunications of the Future" (PE00000001—program "RESTART", project "SPARKS"), by the PNRR project "Tech4You—Technologies for climate change adaptation and quality of life improvement"(ECS 00000009, CUP H23C22000370006, Piano Nazionale di Ripresa e Resilienza), and by Ministero dell'Università e della Ricerca (MUR), Italy, as part of Programma Operativo Nazionale (PON) Ricerca e Innovazione (2014–2020)—Area di Specializzazione AEROSPAZIO.

Conflicts of Interest: The authors declare no conflict of interest.

References

1. Mandelbrot, B.B. *Fractals: Form Chance and Dimension*; W.H. Freeman: San Francisco, CA, USA, 1977.
2. Lauwerier, H. *Fractals—Endless Repeated Geometrical Figures*; Princeton University Press: Princeton, NJ, USA, 1991.
3. Sierpinski, W. Sur une courbe dont tout point est un point de ramification. *CR Acad. Sci.* **1915**, *160*, 302–305.
4. Julia, G. Memoire sur l'iteration des fonctions rationnelles. *J. Pure Appl. Math.* **1918**, *1*, 47–245.
5. Fatou, P. Sur l'itération des fonctions transcendantes entières. *Acta Math.* **1926**, *47*, 337–370. [CrossRef]
6. Mandelbrot, B.B. *The Fractal Geometry of Nature*; W.H. Freeman: New York, NY, USA, 1983.
7. Mandelbrot, B.B. *Fractal and Chaos: The Mandelbrot Set and Beyond*; Springer: New York, NY, USA, 2004.
8. Xinhuan, Y.; Chiochetti, J.; Papadopoulos, D.; Susman, L. Fractal Antenna Elements and Arrays. *Appl. Microw. Wirel.* **1999**, *11*, 34–46.
9. Karmakar, A. Fractal antennas and arrays: A review and recent developments. *Int. J. Microw. Wirel. Technol.* **2021**, *13*, 173–197. [CrossRef]
10. Li, S.J.; Cui, T.J.; Li, Y.B.; Zhang, C.; Li, R.Q.; Cao, X.Y.; Guo, Z.X. Fractal Metasurfaces: Multifunctional and Multiband Fractal Metasurface Based on Inter-Metamolecular Coupling Interaction. *Adv. Theory Simul.* **2019**, *2*, 1970030. [CrossRef]
11. Bayatmaku, N.; Lotfi, P.; Azarmanesh, M.; Soltani, S. Design of Simple Multiband Patch Antenna for Mobile Communication Applications Using New E-Shape Fractal. *IEEE Antennas Wirel. Propag. Lett.* **2011**, *10*, 873–875. [CrossRef]
12. Cohen, N. Fractal antenna applications in wireless telecommunications. In Proceedings of the Electronics Industries Forum of New England, Boston, MA, USA, 6–8 May 1997; pp. 43–49.

13. Anwer, A.I.; Alibakhshikenari, M.; Elwi, T.A.; Virdee, B.S.; Kouhalvandi, L.; Hassain, Z.A.A.; Soruri, M.; Tokan, N.T.; Parchin, N.O.; See, C.H.; et al. Minkowski Based Microwave Resonator for Material Detection over Sub-6 GHz 5G Spectrum. In Proceedings of the 2023 2nd International Conference on 6G Networking (6GNet), Paris, France, 18–20 October 2023; pp. 1–4. [CrossRef]
14. Obaid, S.M.; Elwi, T.A.; Ilyas, M. Fractal Minkowski-Shaped Resonator for Noninvasive Biomedical Measurements: Blood Glucose Test. *Prog. Electromagn. Res. C* **2021**, *107*, 143–156. [CrossRef]
15. Abdulsattar, R.K.; Elwi, T.A.; Abdul Hassain, Z.A. A New Microwave Sensor Based on the Moore Fractal Structure to Detect Water Content in Crude Oil. *Sensors* **2021**, *21*, 7143. [CrossRef]
16. Silva, C.P.N.; Araujo, J.A.I.; Coutinho, M.S.; Oliveira, M.R.T.; Llamas-Garro, I.; de Melo, M.T. Multi-band microwave sensor based on Hilbert's fractal for dielectric solid material characterization. *J. Electromagn. Waves Appl.* **2021**, *35*, 848–860. [CrossRef]
17. Cavalcanti Filho, P.H.B.; Araujo, J.A.I.; Oliveira, M.R.T.; de Melo, M.T.; Coutinho, M.S.; da Silva, L.M.; Llamas-Garro, I. Planar Sensor for Material Characterization Based on the Sierpinski Fractal Curve. *J. Sens.* **2020**, *2020*, 8830596. [CrossRef]
18. Kim, Y.; Jaggard, D.L. The fractal random array. *Proc. IEEE* **1986**, *74*, 1278–1280. [CrossRef]
19. Cohen, N. Fractal Antennas: Part I. *Commun. Q.* **1995**, *9*, 7–22.
20. Cohen, N. Fractal Antennas: Part 2. *Commun. Q.* **1996**, *6*, 53–66.
21. Fractal Antenna Systems Inc. Available online: https://www.fractenna.com/ (accessed on 27 January 2024).
22. Puente, C.; Romeu, J.; Pous, R.; Garcia, X.; Benítez, F. Fractal Multiband Antenna Based on the Sierpinski Gasket. *IEE Electron. Lett.* **1996**, *32*, 1–2. [CrossRef]
23. Anguera, J.; Borja, C.; Puente, C. Microstrip Fractal-Shaped Antennas: A Review. In Proceedings of the 2nd European Conference on Antennas and Propagation (EuCAP 2007), Edinburgh, UK, 11–16 November 2007; pp. 1–7. [CrossRef]
24. Werner, D.H.; Ganguly, S. An overview of fractal antenna engineering research. *IEEE Antennas Propag. Mag.* **2003**, *45*, 38–57. [CrossRef]
25. Puente, C.; Romeu, J.; Bartolemi, R.; Pous, R. Perturbation of the Sierpinski antenna to allocate operating bands. *IEE Electron. Lett.* **1996**, *32*, 2186–2188. [CrossRef]
26. Puente, C.; Romeu, J.; Pous, R.; Cardama, A. On the behavior of the Sierpinski multiband fractal antenna. *IEEE Trans. Antennas Propag.* **1998**, *46*, 517–524. [CrossRef]
27. Baliarda, C.P.; Romeu, J.; Cardama, A. The Koch monopole: A small fractal antenna. *IEEE Trans. Antennas Propag.* **2000**, *48*, 1773–1781. [CrossRef]
28. Bakytbekov, A.; Maza, A.R.; Nafe, M.; Shamim, A. Fully inkjet printed wide band cantor fractal antenna for RF energy harvesting application. In Proceedings of the 11th European Conference on Antennas and Propagation (EUCAP), Paris, France, 19–24 March 2017; pp. 489–491. [CrossRef]
29. Anguera, J.; Andújar, A.; Jayasinghe, J.; Chakravarthy, V.V.S.S.S.; Chowdary, P.S.R.; Pijoan, J.L.; Ali, T.; Cattani, C. Fractal Antennas: An Historical Perspective. *Fractal Fract.* **2020**, *4*, 3. [CrossRef]
30. Anguera, J.; Puente, C.; Martínez, E.; Rozan, E. The fractal Hilbert monopole: A two-dimensional wire. *Microw. Opt. Technol. Lett.* **2003**, *36*, 102–104. [CrossRef]
31. Anguera, J.; Andújar, A.; Benavente, S.; Jayasinghe, J.; Kahng, S. High-directivity microstrip antenna with Mandelbrot fractal boundary. *IET Microw. Antennas Propag.* **2018**, *12*, 569–575. [CrossRef]
32. Borja, C.; Font, G.; Blanch, S.; Romeu, J. High directivity fractal boundary microstrip patch antenna. *Electron. Lett.* **2000**, *36*, 778–779. [CrossRef]
33. Costanzo, S.; Venneri, F.; Di Massa, G.; Borgia, A.; Costanzo, A.; Raffo, A. Fractal Reflectarray Antennas: State of Art and New Opportunities. *Int. J. Antennas Propag.* **2016**, *2016*, 7165143. [CrossRef]
34. Huang, J.; Encinar, J. *Reflectarray Antennas*; Wiley-IEEE Press: New York, NY, USA, 2008.
35. Nayeri, P.; Yang, F.; Elsherbeni, A.Z. *Reflectarray Antennas: Theory, Designs, and Applications*; Wiley-IEEE Press: New York, NY, USA, 2018. [CrossRef]
36. Costanzo, S.; Venneri, F.; Di Massa, G. Bandwidth enhancement of aperture-coupled reflectarrays. *IEE Electron. Lett.* **2006**, *42*, 1320–1322. [CrossRef]
37. Venneri, F.; Costanzo, S.; Di Massa, G. Bandwidth behavior of closely spaced aperture-coupled reflectarrays. *Int. J. Antennas Propag.* **2012**, *2012*, 846017. [CrossRef]
38. Venneri, F.; Costanzo, S.; Di Massa, G. Design and Validation of a Reconfigurable Single Varactor-Tuned Reflectarray. *IEEE Trans. Antennas Propag.* **2013**, *61*, 635–645. [CrossRef]
39. Hum, S.V.; Perruisseau-Carrier, J. Reconfigurable reflectarrays and array lenses for dynamic antenna beam control: A review. *IEEE Trans. Antennas Propag.* **2014**, *62*, 183–198. [CrossRef]
40. Nayeri, P.; Yang, F.; Elsherbeni, A.Z. Beam-scanning reflectarray antennas: A technical overview and state of the art. *IEEE Antennas Propag. Mag.* **2015**, *57*, 32–47. [CrossRef]
41. Costanzo, S.; Venneri, F.; Raffo, A.; Di Massa, G. Dual-Layer Single-Varactor Driven Reflectarray Cell for Broad-Band Beam-Steering and Frequency Tunable Applications. *IEEE Access* **2018**, *6*, 71793–71800. [CrossRef]
42. Costanzo, S.; Venneri, F.; Di Massa, G.; Borgia, A.; Raffo, A. Bandwidth performance of reconfigurable reflectarrays: State of art and future challenges. *Radioengineering* **2018**, *27*, 1–9. [CrossRef]
43. Zubir, F.; Rahim, M.K.A. Simulated fractals shape for unit cell reflectarray. In Proceedings of the 2009 Asia Pacific Microwave Conference (APMC '09), Singapore, 7–10 December 2009; pp. 583–586.

44. Sayidmarie, K.H.; Bialkowski, M.E. Fractal unit cells of increased phasing range and low slopes for single-layer microstrip reflectarrays. *IET Microw. Antennas Propag.* **2011**, *5*, 1371–1379. [CrossRef]
45. Oloumi, D.; Ebadi, S.; Kordzadeh, A.; Semnani, A.; Mousavi, P.; Gong, X. Miniaturized reflectarray unit cell using fractal shaped patch-slot configuration. *IEEE Antennas Wirel. Propag. Lett.* **2012**, *11*, 10–13. [CrossRef]
46. Costanzo, S.; Venneri, F. Miniaturized Fractal Reflectarray Element Using Fixed-Size Patch. *IEEE Antennas Wirel. Propag. Lett.* **2014**, *13*, 1437–1440. [CrossRef]
47. Costanzo, S.; Venneri, F.; Di Massa, G. Modified Minkowski fractal unit cell for reflectarrays with low sensitivity to mutual coupling effects. *Int. J. Antennas Propag.* **2019**, *2019*, 4890710. [CrossRef]
48. Öztürk, E.; Saka, B. Multilayer Minkowski Reflectarray Antenna With Improved Phase Performance. *IEEE Trans. Antennas Propag.* **2021**, *69*, 8961–8966. [CrossRef]
49. Costanzo, S.; Venneri, F.; Borgia, A.; Di Massa, G. A single-layer dual-band reflectarray cell for 5G communication systems. *Int. J. Antennas Propag.* **2019**, *2019*, 9479010. [CrossRef]
50. Costanzo, S.; Venneri, F.; Borgia, A.; Di Massa, G. Dual-Band Dual-Linear Polarization Reflectarray for mmWaves/5G Applications. *IEEE Access* **2020**, *8*, 78183–78192. [CrossRef]
51. Cohen, N. Radiative Transfer and Power Control with Fractal Metamaterial and Plasmonics. U.S. Patent 9,482,474-B2, 1 November 2016. Available online: https://ppubs.uspto.gov/dirsearch-public/print/downloadPdf/9482474 (accessed on 1 March 2024).
52. Cohen, N.; Salkind, P. Enhanced Gain Antenna Systems Employing Fractal Metamaterials. U.S. Patent 11,268,771-B2, 8 March 2022. Available online: https://ppubs.uspto.gov/dirsearch-public/print/downloadPdf/11268771 (accessed on 1 March 2024).
53. Venneri, F.; Costanzo, S.; Di Massa, G. Fractal-Shaped Metamaterial Absorbers for Multireflections Mitigation in the UHF Band. *IEEE Antennas Wirel. Propag. Lett.* **2018**, *17*, 255–258. [CrossRef]
54. Venneri, F.; Costanzo, S.; Borgia, A. A Dual-Band Compact Metamaterial Absorber with Fractal Geometry. *Electronics* **2019**, *8*, 879. [CrossRef]
55. Costanzo, S.; Venneri, F. Polarization-Insensitive Fractal Metamaterial Surface for Energy Harvesting in IoT Applications. *Electronics* **2020**, *9*, 959. [CrossRef]
56. Jiang, H.; Xue, Z.; Li, W.; Ren, W. Multiband polarisation insensitive metamaterial absorber based on circular fractal structure. *IET Microw. Antennas Propag.* **2016**, *10*, 1141–1145. [CrossRef]
57. Amiri, M.; Tofigh, F.; Shariati, N.; Lipman, J.; Abolhasan, M. Miniature tri-wideband Sierpinski–Minkowski fractals metamaterial perfect absorber. *IET Microw. Antennas Propag.* **2019**, *13*, 991–996. [CrossRef]
58. Goyal, N.; Panwar, R. Minkowski inspired circular fractal metamaterial microwave absorber for multiband applications. *Appl. Phys. A* **2023**, *129*, 293. [CrossRef]
59. Xu, H.X.; Wang, G.M.; Qi, M.Q.; Liang, J.G.; Gong, J.Q.; Xu, Z.M. Triple-band polarization-insensitive wide-angle ultra-miniature metamaterial transmission line absorber. *Phys. Rev. B* **2012**, *86*, 205104. [CrossRef]
60. Landy, N.I.; Sajuyigbe, S.; Mock, J.J.; Smith, D.R.; Padilla, W.J. Perfect metamaterial absorber. *Phys. Rev. Lett.* **2008**, *100*, 207402. [CrossRef]
61. Watts, C.M.; Liu, X.; Padilla, W.J. Metamaterial electromagnetic wave absorbers. *Adv. Mater.* **2012**, *24*, 98–120. [CrossRef] [PubMed]
62. Abdulkarim, Y.I.; Mohanty, A.; Acharya, O.P.; Appasani, B.; Khan, M.S.; Mohapatra, S.K.; Muhammadsharif, F.F.; Dong, J. A Review on Metamaterial Absorbers: Microwave to Optical. *Front. Phys.* **2022**, *10*, 893791. [CrossRef]
63. Liang, Y.; Lin, H.; Lin, S.; Wu, J.; Li, W.; Meng, F.; Yang, Y.; Huang, X.; Jia, B.; Kivshar, Y. Hybrid anisotropic plasmonic metasurfaces with multiple resonances of focused light beams. *Nano Lett.* **2021**, *21*, 8917–8923. [CrossRef]
64. Stewart, J.W.; Nebabu, T.; Mikkelsen, M.H. Control of Nanoscale Heat Generation with Lithography-Free Metasurface Absorbers. *Nano Lett.* **2022**, *22*, 5151–5157. [CrossRef]
65. Kim, S.; Vyas, R.; Bito, J.; Niotaki, K.; Collado, A.; Georgiadis, A.; Tentzeris, M.M. Ambient RF Energy-Harvesting Technologies for Self-Sustainable Standalone Wireless Sensor Platforms. *Proc. IEEE* **2014**, *102*, 1649–1666. [CrossRef]
66. Ramahi, O.M.; Almoneef, T.S.; AlShareef, M.; Boybay, M.S. Metamaterial particles for electromagnetic energy harvesting. *Appl. Phys. Lett.* **2012**, *101*, 173903. [CrossRef]
67. Amer, A.A.G.; Sapuan, S.Z.; Nasimuddin, N.; Alphones, A.; Zinal, N.B. A Comprehensive Review of Metasurface Structures Suitable for RF Energy Harvesting. *IEEE Access* **2020**, *8*, 76433–76452. [CrossRef]
68. Sherazi, H.H.R.; Zorbas, D.; O'Flynn, B. A Comprehensive Survey on RF Energy Harvesting: Applications and Performance Determinants. *Sensors* **2022**, *22*, 2990. [CrossRef] [PubMed]
69. Góra, P.; Łopato, P. Metamaterials' Application in Sustainable Technologies and an Introduction to Their Influence on Energy Harvesting Devices. *Appl. Sci.* **2023**, *13*, 7742. [CrossRef]
70. Yogesh, N.; Ouyang, Z. Metamaterial frequency selective surfaces as polarizers. In *Handbook of Metamaterial-Derived Frequency Selective Surfaces. Metamaterials Science and Technology*; Narayan, S., Kesavan, A., Eds.; Springer: Singapore, 2022; Volume 3, pp. 285–311.
71. Xu, H.X.; Wang, G.M.; Qi, M.Q.; Cai, T.; Cui, T.J. Compact dual-band circular polarizer using twisted Hilbert-shaped chiral metamaterial. *Opt. Express* **2013**, *21*, 24912–24921. [CrossRef] [PubMed]
72. Bilal, R.M.H.; Baqir, M.A.; Choudhury, P.K.; Ali, M.M.; Rahim, A.A. On the specially designed fractal metasurface-based dual-polarization converter in the THz regime. *Results Phys.* **2020**, *19*, 103358. [CrossRef]

73. Palandoken, M.; Grede, A.; Henke, H. Broadband microstrip antenna with left-handed metamaterials. *IEEE Trans. Antennas Propag.* **2009**, *57*, 331–338. [CrossRef]
74. Kossiavas, C.; Zeitler, A.; Clementi, G.; Migliaccio, C.; Staraj, R.; Kossiavas, G. X-Band circularly polarized antenna gain enhancement with metamaterials. *Microw. Opt. Technol. Lett.* **2011**, *53*, 1911–1915. [CrossRef]
75. Dong, Y.D.; Toyao, H.; Itoh, T. Compact circularly-polarized patch antenna loaded with metamaterial structures. *IEEE Trans. Antennas Propag.* **2011**, *59*, 4329–4333. [CrossRef]
76. de Fátima Linhares de Vasconcelos, C.; de Albuquerque, M.R.M.L.; da Silva, S.G.; de Ribamar Silva Oliveira, J.; d'Assunção, A.G. Full-wave analysis of annular ring microstrip antenna on metamaterial. *IEEE Trans. Magn.* **2011**, *47*, 1110–1113. [CrossRef]
77. Buell, K.; Mosallaei, H.; Sarabandi, K. A substrate for small patch antennas providing tunable miniaturization factors. *IEEE Trans. Microw. Theory Tech.* **2006**, *54*, 135–146. [CrossRef]
78. Chillakuru, S.R.; Muraleedharan, N.; Upadhayay, M.D. Triangular metamaterial loaded antenna for low RCS stealth application. In Proceedings of the 2022 International Conference for Advancement in Technology (ICONAT), Goa, India, 21–22 January 2022; pp. 1–7.
79. Xu, H.X.; Wang, G.M.; Qi, M.Q. Hilbert-shaped magnetic waveguided metamaterials for electromagnetic coupling reduction of microstrip antenna array. *IEEE Trans. Magn.* **2013**, *49*, 1526–1529. [CrossRef]
80. Assimonis, S.D.; Yioultsis, T.V.; Antonopoulos, C.S. Computational investigation and design of planar EBG structures for coupling reduction in antenna applications. *IEEE Trans. Magn.* **2012**, *48*, 771–774. [CrossRef]
81. Xu, H.X.; Wang, G.M.; Liang, J.G.; Qi, M.Q.; Gao, X. Compact circularly polarized antennas combining meta-surfaces and strong space-filling meta-resonators. *IEEE Trans. Antennas Propag.* **2013**, *61*, 3442–3450. [CrossRef]
82. Liu, G.; Xu, L.; Wu, Z. Miniaturized Circularly Polarized Microstrip RFID Antenna Using Fractal Metamaterial. *Int. J. Antennas Propag.* **2013**, *2013*, 781357. [CrossRef]
83. Xu, H.X.; Wang, G.M.; Qi, M.Q.; Cai, T. Compact fractal left-handed structures for improved cross-polarization radiation pattern. *IEEE Trans. Antennas Propag.* **2014**, *62*, 546–554. [CrossRef]
84. Xu, H.X.; Wang, G.M.; Qi, M.Q.; Zeng, H.Y. Ultra-small single negative electric metamaterials for electromagnetic coupling reduction of microstrip antenna array. *Opt. Exp.* **2012**, *20*, 21968–21976. [CrossRef] [PubMed]
85. Cai, T.; Wang, G.M.; Zhang, X.F.; Shi, J.P. Low-profile compact circularly-polarized antenna based on fractal metasurface and fractal resonator. *IEEE Antennas Wirel. Propag. Lett.* **2015**, *14*, 1072–1076. [CrossRef]
86. Tang, W.; Chen, J.; Cui, T.J. Metamaterial lenses and their applications at microwave frequencies. *Adv. Photonics Res.* **2021**, *2*, 2100001. [CrossRef]
87. Lee, J.; Kim, H.; Oh, J. Large-Aperture Metamaterial Lens Antenna for Multi-Layer MIMO Transmission for 6G. *IEEE Access* **2022**, *10*, 20486–20495. [CrossRef]
88. Xu, H.X.; Wang, G.M.; Qi, M.Q.; Li, L.; Cui, T. Three-Dimensional Super Lens Composed of Fractal Left-Handed Materials. *Adv. Opt. Mater.* **2013**, *1*, 495–502. [CrossRef]
89. Xu, H.X.; Wang, G.M.; Tao, Z.; Cai, T. High-Directivity Emissions with Flexible Beam Numbers and Beam Directions Using Gradient-Refractive-Index Fractal Metamaterial. *Sci. Rep.* **2014**, *4*, 5744. [CrossRef] [PubMed]
90. Xu, H.X.; Wang, G.M.; Tao, Z.; Cai, T. An Octave-Bandwidth Half Maxwell Fish-Eye Lens Antenna Using Three-Dimensional Gradient-Index Fractal Metamaterials. *IEEE Trans. Antennas Propag.* **2014**, *62*, 4823–4828. [CrossRef]
91. Cohen, N.; Okoro, O.; Salkind, P. Wideband Electromagnetic Cloaking Systems. U.S. Patent 10,027,033, 17 July 2018. Available online: https://ppubs.uspto.gov/dirsearch-public/print/downloadPdf/10027033 (accessed on 6 March 2024).
92. Wu, R.; Dong, J.; Wang, M. Wearable Polarization Conversion Metasurface MIMO Antenna for Biomedical Applications in 5 GHz WBAN. *Biosensors* **2023**, *13*, 73. [CrossRef]
93. Althuwayb, A.A.; Alibakhshikenari, M.; Virdee, B.S.; Rashid, N.; Kaaniche, K.; Ben Atitallah, A.; Armghan, A.; Elhamrawy, O.I.; See, C.H.; Falcone, F. Metasurface-Inspired Flexible Wearable MIMO Antenna Array for Wireless Body Area Network Applications and Biomedical Telemetry Devices. *IEEE Access* **2013**, *11*, 1039–1056. [CrossRef]
94. Ozpinar, H.; Aksimsek, S. Fractal interwoven resonator based penta-band metamaterial absorbers for THz sensing and imaging. *Sci. Rep.* **2022**, *12*, 19758. [CrossRef] [PubMed]
95. Zhang, W.; Lin, J.; Yuan, Z.; Lin, Y.; Shang, W.; Chin, L.K.; Zhang, M. Terahertz Metamaterials for Biosensing Applications: A Review. *Biosensors* **2024**, *14*, 3. [CrossRef]
96. Buonanno, G.; Costanzo, S.; Solimene, R. Broadband statistically designed thinned-binned array antennas. *IEEE Trans. Antennas Propag.* **2023**, *71*, 2454–2466. [CrossRef]
97. Buonanno, G.; Solimene, R. Global characterization of linear statistically thinned antenna arrays. *IEEE Access* **2021**, *9*, 119629–119640. [CrossRef]